JOURNAL OF GEOPHYSICAL RESEARCH, VOL. 97, NO. B11, PAGES 15,113–15,128, OCTOBER 10, 1992

Very Long Period Magnetotellurics at Tucson Observatory: Estimation of Impedances

GARY D. EGBERT

College of Oceanography, Oregon State University, Corvallis

JOHN R. BOOKER

Geophysics Program AK-50, University of Washington, Seattle

ADAM SCHULTZ[1]

School of Oceanography, WB-10, University of Washington, Seattle

Eleven years (1932-1942) of electric potential and magnetic measurements at the Tucson observatory represent a unique very long period magnetotelluric (MT) data set. We report here on a careful reanalysis of this data using modern processing techniques. We have developed and used novel methods for separating out the quasi-periodic daily variation fields and for cleaning up outliers and filling in missing data in the time domain. MT impedance tensors, estimated using the cleaned and filled data and using robust frequency domain methods, are well determined and smoothly varying for periods between 4 hours and 10 days. At longer periods the electric field data are swamped by large-amplitude incoherent noise, particularly after the third year of the experiment. Although we find no evidence for contamination of any field components by oceanic motional induction at tidal periods, the MT impedance estimates do show evidence of small systematic biases due to finite spatial scale geomagnetic sources at harmonics of the daily variation period. These periods are thus removed from the time series and not used in further analysis. We show that the resulting impedance tensor is well modeled by a real, frequency-independent distortion of a scalar impedance, which is consistent with non-inductive distortion of the electric fields by local surface geology. To estimate the undetermined static shift of the MT impedance, we compare the long-period MT results to equivalent MT impedances determined from 46 years of geomagnetic data. Combining the geomagnetic and undistorted MT impedances results in scalar impedance estimates for periods $0.17 < T < 91$ days of unprecedented precision. However, for periods less than one day, the phase and amplitude of this impedance, while individually consistent, are not mutually consistent with any one-dimensional conductivity distribution. The inconsistency probably results from a combination of subtle multidimensional effects and systematic biases.

1. INTRODUCTION

From March 1931 to February 1943, the electric potentials on two long (60-90 km), roughly perpendicular lines emanating from the Tucson magnetic observatory were continuously recorded in a cooperative experiment undertaken by the United States Coast and Geodetic Survey, the Bell Telephone Company, and the Department of Terrestrial Magnetism of the Carnegie Institute of Washington [*Rooney,* 1949]. Together with the magnetic field variations recorded at the Tucson observatory, these observations represent a unique very long period magnetotelluric (MT) data set. Several attempts to use this data to infer the electrical conductivity of the Earth's crust and upper mantle have already been reported. In his seminal paper on magnetotellurics, *Tikhonov* [1950] (see also *Tikhonov and Shaksuvarov* [1952]) used amplitudes and phases of daily variation fields from the Tucson data to illustrate the MT method. Subsequently, *Larsen* [1977, 1980] presented results from more detailed and careful analysis of this data. However, recent years have seen advances in all phases of processing and inversion of MT data, suggesting that a reexamination of the Tucson data would be profitable. In this paper we discuss the results of our recent efforts to reanalyze the time series data using modern data processing techniques. A companion paper [*Egbert and Booker*, this issue] examines the implications of the resultant MT impedances for mantle structure.

2. DATA

The MT data analyzed consist of 96,420 hourly mean values of electric and magnetic fields recorded at the Tucson geomagnetic observatory. Electric fields were measured by an approximately L-shaped array with a common electrode located near the observatory (Figure 1). In this paper we use a right-handed coordinate system with x and y aligned along geomagnetic north and east, with z positive down. Magnetic field components, impedance tensors, and other parameters are always expressed in this coordinate system. It will also often be useful to refer to the components of the electric fields E_n and E_e corresponding to the non-orthogonal measurement coordinate system. Approximately 4% of the electric field records are missing, mostly during geomagnetic disturbances which forced the recording galvanometer off scale [*Rooney,* 1949; *Larsen,* 1980]. Thus, while the magnetic time series are essentially complete, there are many small gaps in the electric field time series. These gaps were filled by predicting the electric from the magnetic fields using a procedure to be discussed in detail later.

A typical 50 day section of hourly means of all five components is plotted in Figure 2. The electric fields, which at the scale plotted appear very clean, are strongly dominated by the quasi-periodic daily variation. Indeed, the primary purpose of the

[1] Now at Institute of Theoretical Geophysics, Department of Earth Sciences, University of Cambridge, England.

Paper number 92JB01252.
0148-0227/92/92JB-01252$05.00

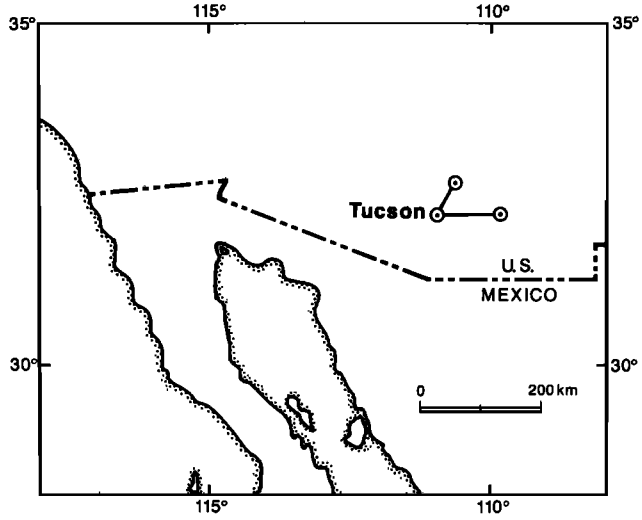

Fig. 1. Location map with electrode array shown actual size.

Tucson experiment was to study diurnal variations of electric fields [*Rooney*, 1949], Because of the importance of the diurnal effects on this data, we will express periods in units of days, and frequencies in units of cycles per day (cpd) throughout this paper. These diurnal fields are best developed during geomagneticaly quiet times and have historically been called solar quiet day variations (S_q). We shall call them S_{dv} (for solar daily variation) to emphasize that we are not restricting attention to time windows of low solar activity.

The dominance of the diurnal signal is also clear in the power spectral densities plotted in Figure 3. There are prominent peaks at the fundamental period of one day and at the first five harmonics for all components. For the H_y and H_z components of the magnetic field, peaks above the background spectra are evident for higher harmonics. There is also clear evidence for lunar tidal effects. For all components the peak at 2 cpd is split, with a second peak occurring at 1.94 cpd. This agrees, within the resolution of the spectrum (0.01 cpd), with the M_2 tidal frequency (1.932 cpd). Although a small portion of this signal could be due to motional induction by tides in the oceans, ionospheric tidal effects are almost certainly of much greater importance. To see this, note that peaks for the higher harmonics of S_{dv} are also split (up to 6 cpd for the vertical magnetic component, and 5 cpd for the electric components). Since these prominent secondary peaks for the higher harmonics do not correspond to any significant lines in the tidal forcing spectrum (or in the oceanic tidal spectra [*Melchior*, 1978]), these lines cannot result from motional electromagnetic induction in the ocean. Furthermore, resolvable tidal components (O_1, 1.076 cpd; N_2, 1.896 cpd) of significant amplitude (approximately 20% of M_2 in the East Pacific [*Parke*, 1982]), do not correspond to substantial peaks in the spectra of Figure 3. Very weak peaks in the spectra occur near 1.069 cpd in the two electric components, but these are comparable in scale to the

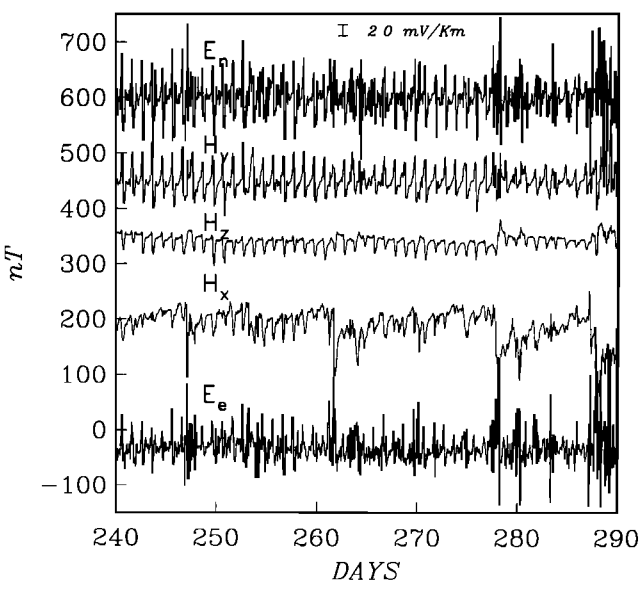

Fig. 2. Fifty days of five-component magnetotelluric data from Tucson. H_x, and H_y, and H_z give the components of the magnetic field variations (in nanoteslas) in a right-handed coordinate system with x geomagnetic north, y geomagnetic east, and z down. E_n and E_e are the electric field variations (millivolts per kilometer) in the measurement coordinate system.

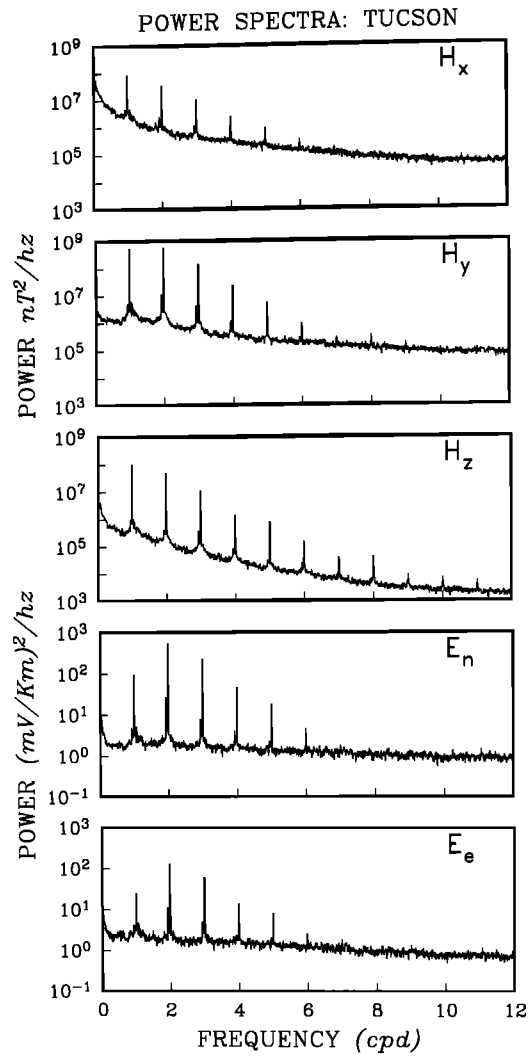

Fig. 3. Power spectra for Tucson magnetotelluric data. After data gaps in the electric field series were filled (using methods discussed in section 4), the time series were divided into 60 2400 point (= 100 days) overlapping segments and multiplied by a time-bandwidth 1 Slepian data taper. Power spectra were then computed by section averaging of the Fourier transformed data. The nominal bandwidth of the estimated spectra is thus 0.01 cpd, and each spectral estimate has 120 degrees of freedom. The prominent diurnal variation peaks have very broad bases and are split with secondary peaks at slightly lower (0.07 cpd) frequencies (see discussion in text).

background oscillations in the spectra and are of dubious significance. There is no evidence of a contribution from N_2 in any component. Because peaks occur in a systematic fashion at nontidal frequencies, and do not necessarily occur at tidal frequencies, it does not seem reasonable to ascribe any significant portion of this signal to oceanic effects.

This conclusion is further substantiated by the occurrence of split peaks in the horizontal magnetic field spectra, since electric currents flowing in the thin oceanic layer would have a negligible effect on horizontal magnetic fields as far inland as Tucson. Indeed, as we will argue more fully below, it is also unlikely that significant motionally induced oceanic electric fields are present in any of these data. We believe that all of the secondary peaks represent modulation of ionospheric/magnetospheric S_{dv} currents by lunar tidal effects. The period of the lunar declinational wave M_f is 13.67 days [*Melchior*, 1978]. In all cases the separation between the split peaks (including the weak secondary peaks near 1 cpd) is 0.07 cpd. This is consistent with a modulation of the S_{dv} with a period of 14±1 days.

It is important to note that the diurnal peaks, while very sharp in the center, cannot be characterized as simple lines. All spectral peaks in Figure 3 are surrounded by broad skirts of increased signal amplitude. For example, the base of the peaks for the north electric field component are 0.15-0.25 cpd wide (much wider than the 0.01 cpd intrinsic resolution of the spectral estimates). This bandwidth corresponds to changes in diurnal variation morphology on time scales of 4-7 days. Examination of the time series confirms the frequent occurrence of this phenomenon. We illustrate this point in Figure 4 where we plot 50 days of raw data and four filtered versions of the east-west component of the magnetic field time series. The trace plotted just below the raw data represents a narrow band estimate of the combined seasonally varying diurnal and tidal signals. To compute this we first estimated the average diurnal signal as a smooth function of local time and day of year (averaged over 11 years). After subtracting

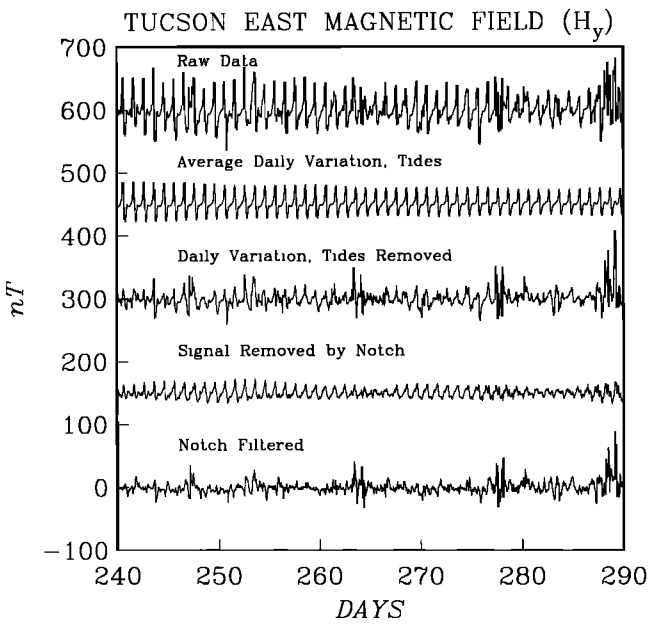

Fig. 4. Fifty days of data for H_y component. From top: raw data; estimated regular daily variation and tidal components; data with daily variation and tides removed still shows evidence of quasi-periodic daily variation; additional signal removed by daily variation notch, showing modulation with a 14 day period and irregular variations of DV signal; notch-filtered signal used for further analysis.

the daily median values for each component, we binned data by hour of the day and time of year. Each bin was 14 days wide, so for the full 11 years of the experiment each bin contained 11×14 = 154 measurements. These were averaged using a robust procedure, and the resulting 24×26 array of averages was fit with a smoothing spline using doubly periodic boundary conditions. This seasonally and diurnally varying signal was then subtracted from the raw data, and the residual was fit with 24 principal oceanic tidal components [*Melchior*, 1978] using a robust linear least squares procedure. The tidal and diurnal signals were then summed to yield the seasonally modulated, nearly periodic second trace of Figure 4. The residual left after this narrow band signal is subtracted from the raw data is the third trace. It still has an obvious, albeit irregular, diurnal signal. To remove this we resorted to a notch filter, constructed to remove signal in bands centered at periods of i cpd, $i = 1, 12$. The filter was 168 points (= 7 days) in length and had a nominal notch width of 0.15 cpd, with notches centered at each harmonic of one day. The final filtered time series and the signal removed by the notch are plotted at the bottom of Figure 4. The signal removed by the notch shows clear evidence of the 14 day modulation suggested by the secondary peaks in the power spectra, as well as the more rapid changes in diurnal signal form which are responsible for broadening the S_{dv} peak.

The bandwidth of the S_{dv} signal is important for our purposes since, as we shall show (see also *Larsen* [1975]), transfer functions computed at S_{dv} frequencies show evidence of systematic biases. Thus, except in the next section, where we illustrate the effect of the S_{dv} signal on transfer function estimates, further analysis focuses on the continuum signal in bands between the lines and is based on the notch-filtered time series. The processing to this point can then be thought of as prewhitening to suppress leakage of the S_{dv} lines and their skirts into these intermediate bands.

One other feature to note in the power spectra of Figure 3 is the rapid rise in spectral density for the electric components at the very left edge of the plot at frequencies below 0.1 cpd. The character of the long-period variations is more clearly evident in the low-passed time series of Figure 5 (0.2 cpd cutoff). The amplitudes of all components are relatively low at the beginning of the experiment and grow to a maximum around 2000-3500 days; after this they decrease. For the magnetic components, this represents solar cycle variations in geomagnetic storm (D_{st}) signals. For the electric fields, however, there is a marked change in character after about day 800 in E_n and after about day 1000 in E_e. Unlike the gradual growth of the magnetic signals, the electric field amplitudes become abruptly larger and the signal appears much more erratic. Furthermore, the relative amplitude variation of the long-period electric field measurements over the course of the experiment is much greater than that seen for the magnetic field measurements. Lack of coherence at long period is clearly evident in Figure 5. Note in particular the very large yearly variation in E_n during the middle of the experiment, which has no counterpart in the magnetic components.

3. IMPEDANCES AND SOURCE EFFECTS

For uniform external sources, the Fourier transformed horizontal electric and magnetic field vectors **E** and **H** satisfy

$$\mathbf{E} = \mathbf{Z}\mathbf{H} \tag{1}$$

where **Z** is the MT impedance tensor. Of course, real data are always contaminated by noise, so this idealized relation can hold

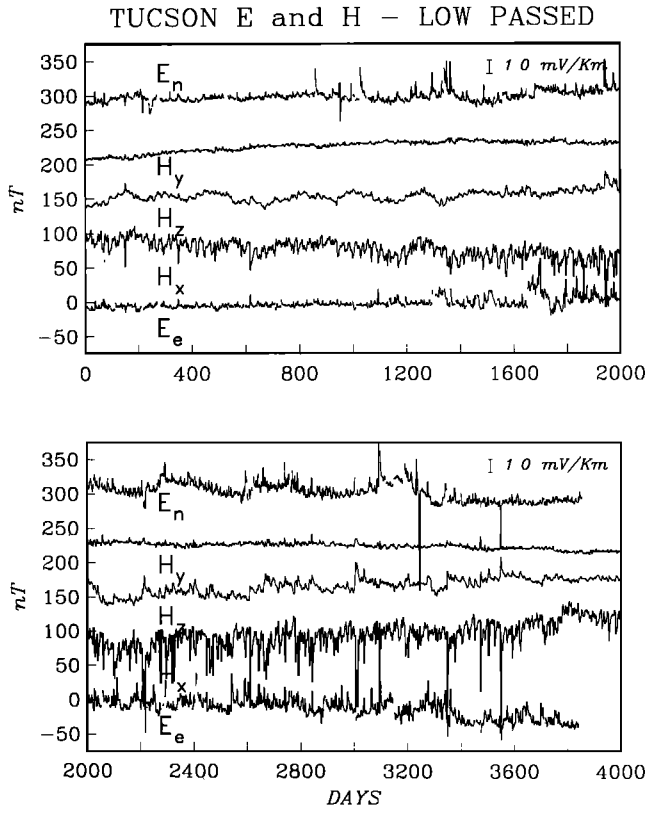

Fig. 5. Low pass filtered magnetotelluric data. Filter is based on a 4π-prolate window with a nominal cutoff (3 db point) of 0.2 cpd. Note the sudden increase in amplitude (and subsequent irregularity) of E_n around day 800 and of E_e around day 1000, while the amplitude of geomagnetic variations (evident mostly in H_x and H_z) gradually increases toward the mid to late portion of the experiment. Also note that the long-period variation in E_n is dominated by a yearly signal, which is not seen in the magnetic fields.

only approximately. Furthermore, the assumption of uniform external sources can never be exactly correct. For physically realistic finite sources, the impedance (which is equal to the ratio of electric to magnetic fields at the measurement location) will depend on the exact spatial configuration of external sources. The utility of the MT method derives from the fact that, provided source wavelengths l are large compared to penetration depths in the Earth δ, the uniform source approximation is quite accurate, with the correction for wavenumber being of the order of $(\delta/l)^2$ [*Waitt*, 1962; *Swift*, 1967; *Madden and Nelson*, 1986]. For the very low frequency (0.1-10.0 cpd) variations considered here, δ ranges from several hundred to perhaps a thousand kilometers, and it is not obvious that the effect of finite source wavelengths will always be negligible. However, there is good evidence that at these periods (excluding harmonics of S_{dv}) typical source length scales at geomagnetic mid-latitudes are 5000-10000 km or more [*Bannister and Gough*, 1978; *Egbert*, 1989; *Banks and Ainsworth*, 1992], while penetration depths do not exceed ≈600–700 km until periods exceed ≈5–10 days. The analysis of *Dmitriev and Berdichevsky* [1979] shows that provided sources are constant or vary linearly over a circle of radius ≈3δ (approximately 2000 km or less for periods below 5 days), the wavenumber dependence of the impedance can be ignored. At longer periods, where penetration depths are greater, external sources can be well approximated as a zonal dipole [*Banks*, 1969; *Schultz and Larsen*, 1983]. It is simple to map the zonal dipole MT impedance for a spherical Earth to the uniform source MT impedance for a flat Earth [*Weidelt*, 1972]. Thus our working hypothesis is that the Tucson **E** and **H** fields generally satisfy (1), but we must allow for the possibility that large deviations may result from sources of unusually small spatial scale (as well as other sources of noise). We must also state at the outset that small biases due to persistent source effects must be considered a possibility in very long period induction data of the sort considered here.

To estimate **Z**, we use a variant of the robust transfer function estimate described by *Egbert and Booker* [1986]. This approach, which downweights "outliers" or unusual data points, has proven effective at reducing source biases in magnetovariational transfer functions. Estimates in the frequency domain are calculated from a series of short, overlapping data segments using a regression M-estimate [*Huber*, 1981]. The estimates in the frequency range 0.5-12 cpd use 10 day (240 point) data segments. Estimates at lower frequencies are obtained from longer (40 or 160 day) segments of low-pass filtered and decimated data. Before transformation with a non-power-of-2 fast Fourier transform, each segment is further prewhitened (using an adaptive autoregressive filter) and multiplied by a time-bandwidth 1 Slepian data taper [*Thomson*, 1977]. For initial exploratory work, we used a combination of band and time averaging to produce robust estimates with bandwidths 5% of the center frequency for periods less than one day, increasing to 50% at 0.025 cpd. Because we found that the transfer functions varied only slowly with frequency, we obtained more precise final estimates using wider bands (10% at frequencies < 1 cpd, increasing to 50% at 0.05 cpd). In all cases, bands did not overlap, so adjacent estimates are at least approximately independent.

The S_{dv} involves moving sources of finite spatial scale. Thus the assumption that the signal is dominated by a uniform source may not be reasonable at S_{dv} frequencies. To explore the possible effects of finite spatial scale sources associated with S_{dv} fields, estimates were first computed for the raw data and for the data with the diurnal and tidal line spectrum removed (both illustrated in Figure 4). Apparent resistivities ρ and impedance phases ϕ were computed from the elements of the complex impedance tensor using

$$\rho_{ij} = \left(\frac{1}{5f}\right)|Z_{ij}|^2$$

and

$$\phi_{ij} = arg(Z_{ij})$$

where f is the frequency (in hertz) and the units of the impedance are millivolts per kilometer per nanotesla. The off-diagonal values are plotted with 1σ standard error bars in Figure 6. The solid and open symbols correspond to estimates obtained from the raw data and from the data with lines removed respectively.

We first discuss the common features, which are also shared by the estimates computed from the notch-filtered data. For $f > 1$ cpd, estimates of both ρ and ϕ have relatively small error bars and vary smoothly with period. However, there are good reasons to discount the shorter-period estimates. Approaching the Nyquist frequency ($f = 12$ cpd) the phases drop smoothly to zero, and apparent resistivities are reduced. Furthermore, the multiple squared coherence (shown for the raw data in Figure 7) which exceeds 0.9 for $6 > f > 1$ cpd, drops dramatically at higher frequencies. This behavior is consistent with severe aliasing in the hand-digitized hourly mean values. We consider estimates for $f \geq 6$ cpd (i.e., half the Nyquist frequency) unreliable and omit them from further consideration.

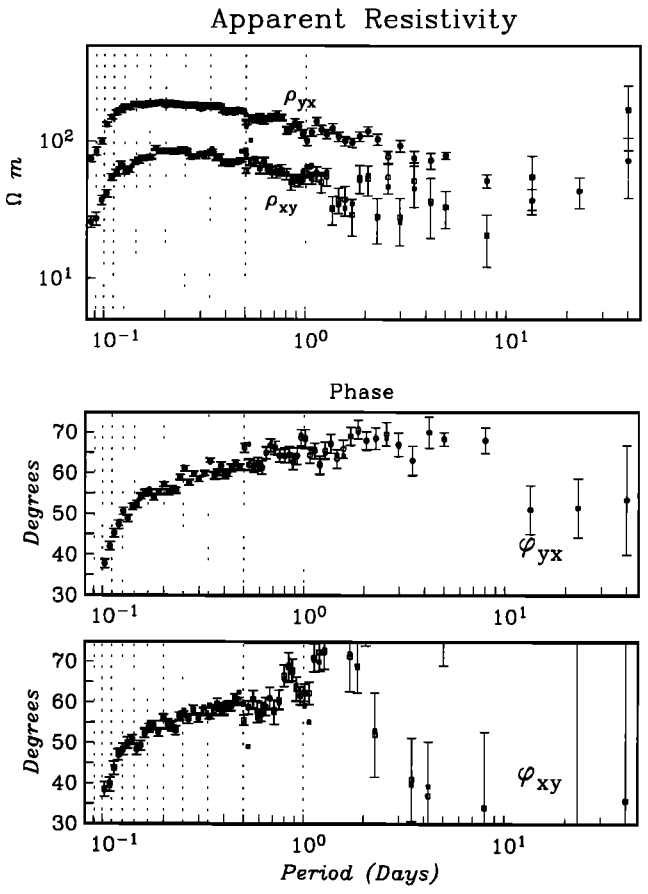

Fig. 6. Apparent resistivity and phase estimates for Tucson magnetotelluric data. Bands are non-overlapping with a width that is 5% of the central frequency, except at longer periods. The coordinate system used is geomagnetic (so the x coordinate is in the direction of geomagnetic north, 9.7° east of true north). Solid symbols are estimates obtained from raw data; open symbols with 1σ error bars represent estimates obtained from data with tidal lines removed. For periods less than one day the apparent resistivity curves are nearly parallel and the phase curves are virtually identical, suggesting the impedance tensor is consistent with a distorted one-dimensional conductivity model. Approaching the Nyquist period ($T = 0.08$ day) the phases drop smoothly to zero, and apparent resistivities are severely reduced. This behavior is consistent with severe aliasing in the hand digitized hourly mean values. At longer periods, only the yx mode, which corresponds to excitation by north-south magnetic sources (denoted by circles) is reasonably well determined. The behavior of the estimates for both modes is also erratic at periods corresponding to the first few harmonics of the daily variation (vertical dashed lines). Removing tidal lines results in some improvements in the estimates (e.g., in ρ_{xy} at 1 and 2 cpd), but problems at daily variation periods remain. In particular, note the systematic upward bias of ϕ_{yx} at i cpd, $i = 1, 6$.

For $1 > f > 0.1$ cpd, only ρ_{yx} and ϕ_{yx} are reasonably well determined. For the orthogonal mode ρ_{xy} and ϕ_{xy} are erratic and have large error bars. The relative quality of the estimates for the two source polarizations largely reflects the difference in magnetic field signal power; for periods beyond one day, the source fields have a dominantly zonal morphology with little signal in the east-west magnetic component [*Banks*, 1969; *Schultz and Larsen*, 1983]. Note that the poor quality of the long-period ρ_{xy} and ϕ_{xy} estimates is not reflected in the coherences, which are very similar for the two modes. This apparent paradox will be explained later when we consider the distortion of the electric field by near-surface structure. The parallel nature of the log apparent resistivity and the near identity of the phase curves, in the period range

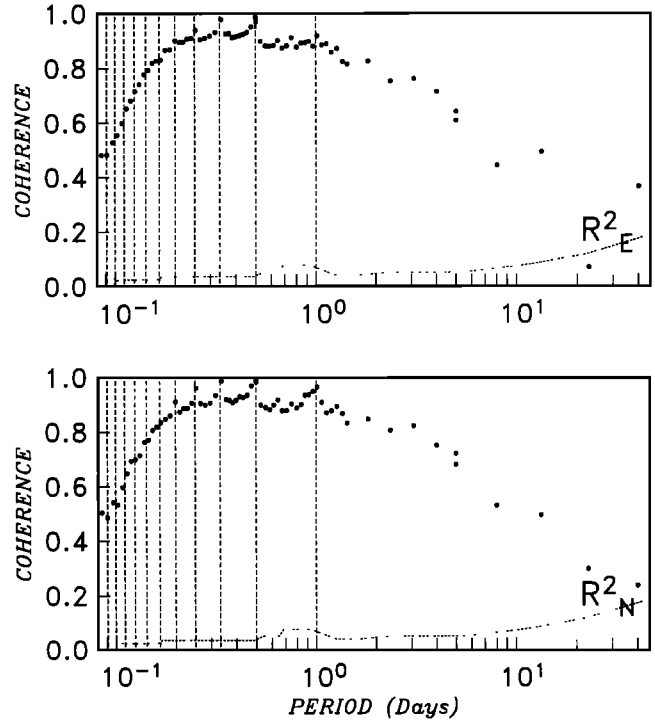

Fig. 7. Multiple squared coherence for electric fields. Note the peaks in coherence at integer multiples of 1 cpd (vertical dashed lines). Dashed curve at bottom is 95% significance level for the squared coherence.

where both modes are well determined, will be discussed in the same context.

For lower frequencies ($f < 0.1$ cpd), the multiple coherence (Figure 7) drops to low values, and estimates for both polarizations contain little or no useful information. Together with our earlier discussion of electric field noise in the time domain, this evidence suggests that the very long-period electric field measurements are completely dominated by noise, most probably resulting from random and seasonally varying electrochemical potentials on the crude (by modern standards) lead wire electrodes [*Rooney*, 1949].

For the raw data, coherence (Figure 7) rises sharply in the vicinity of the first five harmonics of S_{dv}, while the estimated phase and apparent resistivity curves are noticeably erratic at the same frequencies. For these data, large deviations in all responses (solid symbols, Figure 6) are evident at 1 and 2 cpd. In addition, the phase ϕ_{yx} appears to be systematically biased up at 3, 4, 5, and possibly 6 cpd. These biases (of the order of 5-10 degrees) are very significant when compared to the estimation errors. Removal of the tidal and S_{dv} line spectrum reduces the magnitude of the deviations at 1 and 2 cpd (open symbols, Figure 6) but has little effect on the systematic deviations of ϕ_{yx} for higher harmonics of S_{dv}. All reasonable tidal lines have been removed, so it is unlikely that these deviations result from motional induction of electric fields in the ocean. Furthermore, the rise in coherence at the very periods where the estimates become erratic argues against an unusual noise source. We believe that the only reasonable interpretation is that these biases result from the fact that the S_{dv} source has a sufficiently short spatial wavelength that its MT impedances systematically differ from the impedances associated with the larger scale source of the continuum background.

For most of the remainder of this paper we focus on the impedances obtained from the notch-filtered data at frequencies

between the diurnal harmonics. While it is reasonable to assume that the external sources are more nearly uniform at these intermediate frequencies, it is by no means clear that contamination of impedance estimates by unknown variations of source wavenumbers can be neglected anywhere in the period range considered here. Although these effects may be small, resulting in systematic variations of phases of only a few degrees, even small systematic biases can complicate interpretation.

4. PREDICTED AND RESIDUAL ELECTRIC FIELDS

Before proceeding with further interpretation of the estimated impedances, we consider prediction of the electric fields from the essentially complete magnetic field time series. Predicted electric fields were used to fill in short data gaps, to remove isolated outliers in the time domain, and to further study the character of signal and noise in the Tucson MT data. We use a time domain prediction method which is described in more detail by *Egbert* [1992]. The method is similar in philosophy to the procedure for detecting outliers in geomagnetic daily mean value time series discussed by *Schultz and Larsen* [1983].

The electric fields in the time domain can be predicted from the time-domain magnetic field using

$$\mathbf{e}_t = \sum_{t'=-\infty}^{\infty} \mathbf{I}_{t'} \mathbf{h}_{t-t'} ,$$

where the impulse response tensor $\mathbf{I}_t$ is related to the impedance tensor estimate $\hat{\mathbf{Z}}$ at frequency ω via the discrete Fourier transform

$$\hat{\mathbf{Z}}(\omega) = \sum_{t=-\infty}^{\infty} \mathbf{I}_t e^{2\pi i \omega t} + \boldsymbol{\varepsilon} . \tag{2}$$

Note that this discrete impulse response may involve negative lags (i.e., it may not be causal), even in cases (e.g., one-dimensional conductivity [*Weidelt*, 1972]) where the continuous time impulse response must be causal [see *Egbert*, 1992]. For the purpose of filling in short gaps in the electric field data, a pilot estimate of $\hat{\mathbf{Z}}$ is computed from data segments with no gaps in the electric fields. As already noted, our robust processing scheme breaks the time series up into a series of short time segments. Thus computing the pilot estimate simply involves eliminating from consideration any segments containing gaps. There is a complication, however, because we have already concluded that $\mathbf{Z}$ for S_{dv} differs from $\mathbf{Z}$ for the continuum. Since we are interested in the continuum and not the S_{dv} impedances, we seek the discretely sampled impulse response which agrees, over the frequency bands of interest, with the estimated frequency domain continuum impedance tensors. The pilot estimate of the continuum impedance tensor is computed from data segments without gaps, which have had lines removed and been notch filtered in exactly the manner described earlier.

To compute estimates of $\mathbf{I}_t$ from the pilot observed impedances, we used a regularized inversion [*Egbert*, 1992]. Specifically, we find the impulse response $\hat{\mathbf{I}}_t$ whose Fourier transform minimizes

$$\int_0^{\omega_{Nyquist}} d\omega \left\| \frac{d^2 \mathbf{Z}}{d\omega^2} \right\|^2 \tag{3}$$

subject to fitting the observed impedances within their errors. $\hat{\mathbf{I}}$ computed in this way is the impulse response corresponding to a spline smoother (in the frequency domain) of the observed impedances. In practice, it is necessary to truncate the impulse response to a finite time interval. However, the smoothness criteria (3) tends to localize the impulse response in the vicinity of the origin, so a relatively small number of nonzero coefficients in (2) are required to adequately approximate the estimated impedance. This is illustrated in Figure 8, where the impulse response for the Tucson Z_{yx} impedance is plotted.

To fill in missing data in the raw electric field series, we first convolved the magnetic fields with $\hat{\mathbf{I}}$ to predict an electric field time series. The predicted fields were subtracted from the measured fields to form two electric field residual time series. Since the long-period electric fields are known to be incoherent with the magnetic fields and hence cannot be predicted from the magnetic fields, the residual series were low-pass filtered and all data gaps in these smoothed residual series were filled by cubic spline interpolation. Missing data in the original time series were then replaced by the sum of the interpolated long-period electric field residual series, and the electric fields predicted from the magnetic fields. At the same time the residual series were searched for large isolated outliers, which were treated as missing data and replaced. The cleaned and filled time series were reanalyzed in exactly the same manner to improve the predicted field in the gaps. This slightly reduced the error bars but otherwise produced results very similar to the pilot estimates.

We also used the time domain prediction filter in an effort to better understand the character of the noise in the time domain. As an example, consider the predicted and residual time series for the east component of the electric field after it has been subjected to a long-period ($5 \le T \le 25$ days) band-pass filter (Figure 9). The increase in long-period noise in the electric fields during the fourth year of the experiment is very evident in the residual series. This trend in the noise suggests that the earlier data segments should be more heavily weighted. However, several simple ad hoc weighting schemes along these lines made little difference in the results. We can probably conclude that the sources of long-period noise do not degrade the shorter-period signals, but we did not pursue this possible refinement further. Overall, the noise in the time domain does not appear to be dominated by a small number of outliers or unusual events. It thus seems unlikely that any further refinements to the robust estimation techniques that we have employed would result in substantial improvements in estimates. Indeed, standard least squares estimates of the long-period impedances based on the raw data are very similar to the robust estimates based on the cleaned and filled data.

The power spectral density of the east component residuals (Figure 10*a*) is flat except for the prominent peaks associated with

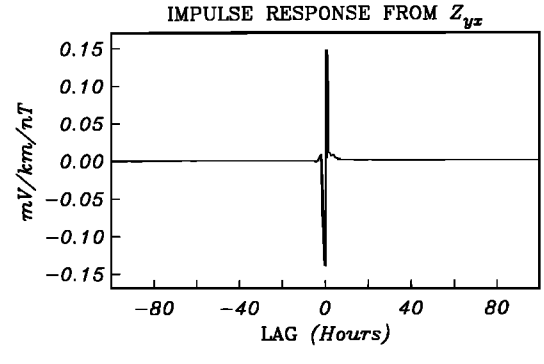

Fig. 8. Impulse response computed for the Z_{yx} component of the Tucson impedance. Note that the impulse response is not causal (i.e., $\mathbf{I}_t \neq 0$ for $t < 0$). $\mathbf{I}_t$, which minimizes the norm of (3) with $n = 2$, is strongly localized in the vicinity of the origin.

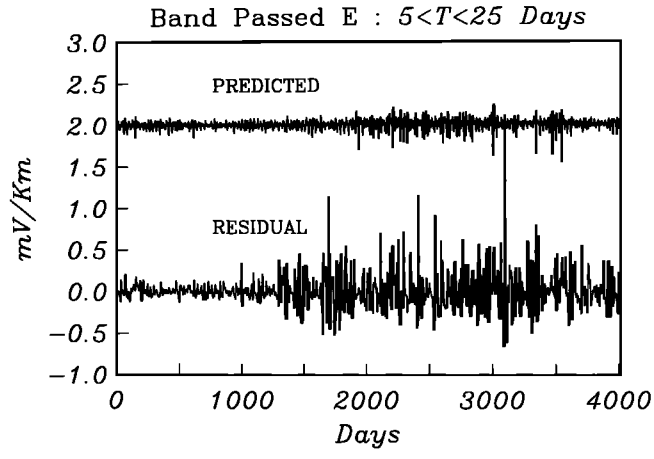

Fig. 9. Predicted and residual parts of the east component of the band-passed ($5 < T < 25$ days) electric field time series. The degradation of the long-period electric field measurements after day 1000 is clearly evident. Noise at these periods is fairly continuous and much larger than the signal.

the S_{dv} and lunar periodicities, and the rise in the spectrum at low frequencies. Note that the first eight harmonics of the S_{dv} can be resolved in the residual spectrum, compared to the total spectrum (Figure 3) where only the first six harmonics show clear evidence of spectral peaks. This difference is presumably due to the fact that the predicted electric field time series contain S_{dv} signals predicted from the magnetic signals by the continuum impedance rather than the S_{dv} impedance and is thus further evidence for distinctly different impedances for the S_{dv} and the continuum. As with the total spectrum, the peaks in the residual spectrum at S_{dv} periods are broad at their base. The lunar lines noted in the total field spectra are also evident in the residual spectrum, as is the sharp increase in noise power at the very lowest frequencies. Results for the north component are very similar and are not shown. The residual spectra reinforce the conclusions reached earlier: source field contamination from S_{dv} fields can be significant in MT data at frequencies up to 8 cpd and is a relatively broadband phenomenon. While the residual spectra suggest that frequencies near solar and lunar periodicities should be avoided, they do not reveal any other surprising noise sources which might be well localized in frequency.

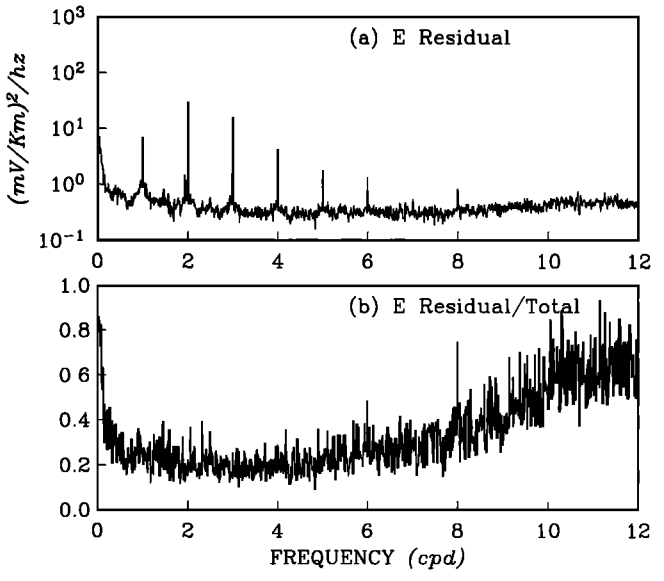

Fig. 10. (*a*) Residual power spectrum for the east-west electric field component (in the measurement coordinate system). The residual spectrum is flat except for the prominent peaks at daily variation and tidal frequencies. Note that peaks in the residual spectrum are evident to frequencies as high as 8 cpd. Note also the steep climb of the residual spectrum at low frequencies. (*b*) Ratio of the residual spectrum of Figure 10*a* to the total spectrum of Figure 3.

An estimate of the fraction of the total power which is noise is equal to one minus the multiple squared coherence (Figure 7). A somewhat different perspective on signal to noise is provided by computing this ratio directly from the estimated residual spectrum (Figure 10*a*) and total spectrum (Figure 3). In this case the estimated noise power is based on the consistency of the observed components with the fields predicted by the estimated time domain impulse response. The impulse response, in turn, corresponds to a smooth frequency domain transfer function, which is fit only to the notch-filtered data. In contrast, the squared coherence gives an estimate of noise based on the consistency of the magnetic and electric fields within narrow frequency bands. As noted in the discussion of Figure 7, the squared coherence has peaks which reach values of 0.95-0.99 at multiples of 1.0 cpd. This demonstrates that noise is small relative to the large S_{dv} signal at these periods. However, the spectral ratio, Figure 10*b* does not show low relative noise amplitudes at S_{dv} periods. This demonstrates that the predicted electric field at S_{dv} periods deviates substantially from the measured signal and proves again that the actual transfer functions at S_{dv} periods must deviate substantially from those interpolated from estimates at intermediate frequencies unaffected by S_{dv}. One other useful piece of information may be gleaned from the spectral ratio plot. If there were significant motional induction by oceanic tides, one would expect enhancement in the spectral ratio estimate of the noise at 1 and 2 cpd (corresponding to the dominant diurnal and semidiurnal solar and lunar tides) relative to the higher harmonics of the S_{dv} which cannot be due to motional induction. This is because motional induction would have a different transfer function than the ionospheric component of S_{dv}. Such behavior is not seen. The spectral ratio is the same at 3 and 4 cpd as it is at 1 and 2, and we have further evidence to rule out oceanic tidal effects.

To compute estimation errors for the transfer functions, a statistical model for the observed electric field data of the form (1) is typically assumed. Furthermore, it is assumed (implicitly, at least) that the electric field noise components represented by the elements of η are uncorrelated. This assumption is probably incorrect more often than not, and it is particularly questionable for the Tucson MT data, where the two electric field channels shared a common electrode. In fact, the full (complex) covariance matrix of η is easily estimated from the frequency domain residual vectors $\mathbf{r} = \mathbf{e} - \hat{\mathbf{Z}}\mathbf{h}$ by

$$\hat{\Sigma}_\eta = \langle \mathbf{r}\mathbf{r}^\dagger \rangle \tag{4}$$

where the brackets denote averaging (over frequencies or time sections), and the dagger denotes the Hermitian conjugate transpose. With Σ_η known or estimated, the full covariance matrix of the impedance tensor elements can be computed using a simple extension of the standard error analysis for linear models. A straightforward calculation shows that covariance of the ij and $i'j'$ elements of the impedance tensor is

$$\Sigma_{(ij)(i'j')} = N^{-1}(\langle \mathbf{h}\mathbf{h}^\dagger \rangle^{-1})_{jj'}(\Sigma_\eta)_{ii'} \tag{5}$$

where N is the number of Fourier coefficients averaged and $\langle \mathbf{h}\mathbf{h}^\dagger \rangle$ is the horizontal magnetic field spectral density matrix.

The asymptotic error estimates for the regression M-estimates [*Huber*, 1981; *Egbert and Booker*, 1986] can then be extended in the obvious way, by simply replacing the residual variance by the full estimated residual covariance.

If all noise were in the electrodes, and noise characteristics of all electrodes were identical (and independent), then, for an L configuration with a shared electrode, the complex correlation between the electric field residuals for the two channels should have a magnitude of ≈ 0.7 and a phase of zero. The observed magnitude for the Tucson MT data is between 0.8 and 0.9, except at the lowest frequencies, where it still exceeds 0.5 (Figure 11). The relatively higher correlation magnitude, and the small but systematically frequency dependent deviation of the phase from zero (particularly for periods $T < 1$ day), suggests other sources of coherent noise (e.g., ionospheric source-related effects). However, the magnitude of the correlation could also be explained if the common electrode was noisier than the other two electrodes.

5. STATIC DISTORTION

Over their entire useful period range the apparent resistivity curves ρ_{xy} and ρ_{yx} are very close to parallel, while the phases ϕ_{xy} and ϕ_{yx} are nearly identical (Figure 6). This suggests that the impedance may be consistent with a one-dimensional conductivity model, complicated by near-surface, non-inductive distortion of the electric field. If this is so, the elements of the full impedance tensor, estimated at periods $T_1, T_2, \cdots, T_K$, can be written

$$Z_{ij}(T_k) = D_{ij}\, Z_0(T_k), \tag{6}$$

where $Z_0(T)$ is the undistorted scalar one-dimensional impedance, and D_{ij}, $i, j = 1, 2$ are real, period-independent distortion parameters [e.g., *Larsen*, 1977].

The estimated impedance elements determine $Z_0(T_k)$ and D_{ij} only up to an arbitrary (period independent) multiplicative constant [*Larsen*, 1977, 1980]. Additional information, such as an independent undistorted estimate of the impedance at one or more periods, is required to eliminate this scale ambiguity. We thus estimate the undistorted scalar impedance in two steps. We first fix the unknown scale factor (e.g., by assuming that D_{12}=1), and then find the remaining three real elements of the distortion matrix **D**, together with the set of scalar impedances $Z_0(T_k)$ which best fit the estimated impedance tensors $\hat{\mathbf{Z}}(T_k)$. Then, as suggested by *Larsen* [1980], we use equivalent MT impedances estimated from long-period magnetic observatory data [*Larsen*, 1980; *Schultz and Larsen*, 1987] to estimate the true scale of the distortion (D_{12}) and the undistorted scalar impedances. The first step in this procedure, covered in this section, allows us to optimally combine all of the information in the impedance tensors into a single scalar impedance curve with the smallest possible estimation errors. It also allows a simple initial test of the adequacy of the distorted one-dimensional conductivity model: Can complex scalars $Z_0(T_k)$ and a real matrix **D** be found which reproduce the observed impedances within their errors? Note that this initial test of goodness of fit does not address the question of whether the resulting scalar impedance estimates $Z_0(T_k)$ are consistent with any one-dimensional conductivity model. This second question can be answered with the D^+ inversion of *Parker* [1980] and *Parker and Whaler* [1981] and will be considered in the next section.

Finding the distortion matrix elements and scalar impedances which best fit the estimated impedance tensors requires solution of a simple nonlinear least squares problem. It is convenient to write the distortion parameters and the impedance tensors as real and complex vectors, respectively, which we denote as bold lower case letters:

$$\mathbf{d} = [D_{11}\ D_{21}\ D_{12}\ D_{22}]^T$$

and

$$\hat{\mathbf{z}}_k = [\hat{Z}_{11}(T_k)\ \hat{Z}_{21}(T_k)\ \hat{Z}_{12}(T_k)\ \hat{Z}_{22}(T_k)]^T .$$

Using this notation and allowing for errors in the estimated impedances, (6) becomes

$$\hat{\mathbf{z}}_k = \mathbf{d}Z_0(T_k) + \varepsilon_k \qquad k = 1, K \tag{7}$$

where the estimation error vectors $\varepsilon_k = (\varepsilon_{11k}\ \varepsilon_{21k}\ \varepsilon_{12k}\ \varepsilon_{22k})$ have covariance matrices

$$\mathrm{Cov}(\varepsilon_k) = \Sigma_k,$$

which can be estimated using (5). To estimate the parameters **d** and $Z_0(T_k)$, $k = 1, K$, we minimize the weighted residual sum of squares

$$\mathbf{J} = \sum_k \mathbf{J}_k = \sum_k (\mathbf{z}_k - \mathbf{d}Z_0(T_k))^{\dagger} \Sigma_k^{-1} (\mathbf{z}_k - \mathbf{d}Z_0(T_k)) . \tag{8}$$

A more detailed discussion of this minimization problem is given in the appendix, where we also derive a simple approximation for the estimation error variances.

Figure 12 plots the full estimated impedance tensors $\hat{\mathbf{Z}}(T_k)$ (with 1σ standard error bars), along with the corresponding components of the predicted impedances $\hat{\mathbf{d}}\hat{Z}_0(T_k)$. Qualitatively, the simple distorted scalar impedance (with $2K+1 = 49$ free parameters) appears to provide a very good fit to the unconstrained full impedance tensors (which consist of a total of $8K = 184$ independent real numbers). The undistorted one-dimensional impedance, Z_0, is essentially a weighted average over all four elements of **Z** and thus has smaller error bars, and is smoother than, any of the individual elements. Consequently, the predicted impedance

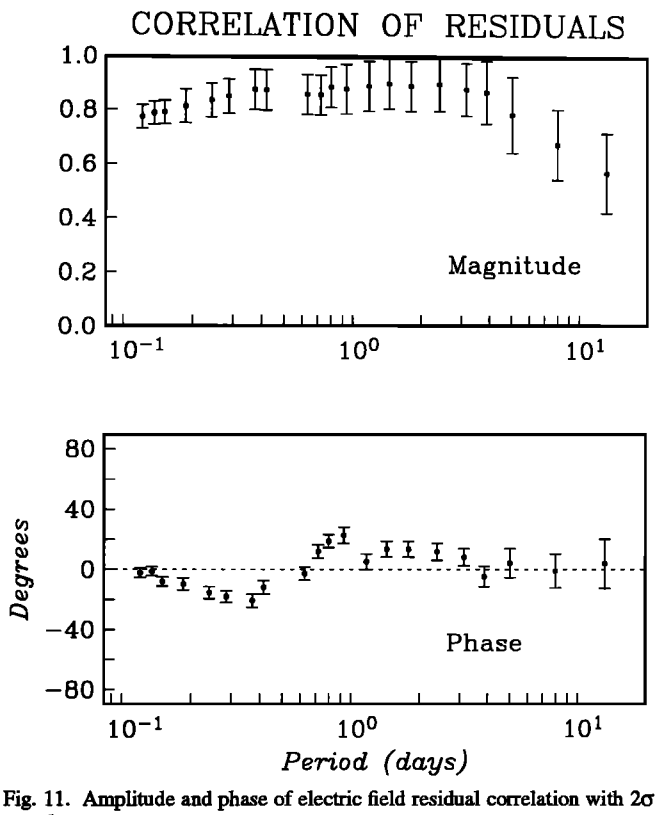

Fig. 11. Amplitude and phase of electric field residual correlation with 2σ error bars.

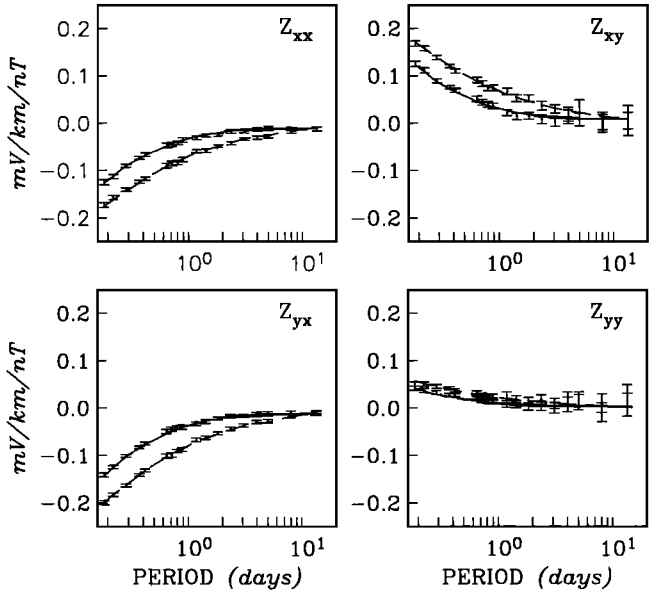

Fig. 12. Impedance tensors estimated (plotted with one-sigma error bars) and computed from best fitting distorted scalar impedance model (continuous curves). Qualitatively, the simple one-dimensional model fits quite well.

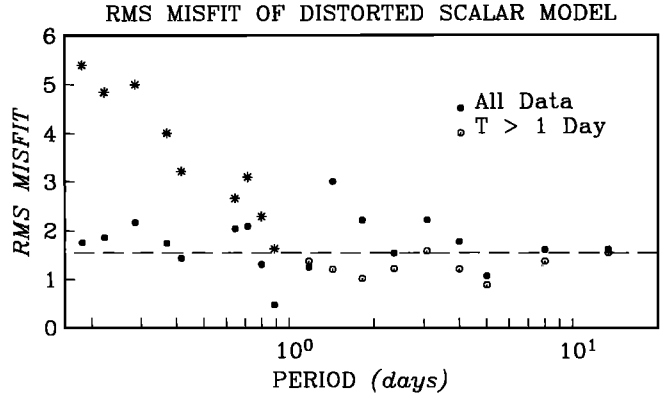

Fig. 13. RMS misfits ($(J_k/3)^{1/2}$) of distorted scalar model versus period. When impedances for the full period range are used to estimate the distortion parameters (sold circles), misfits are systematically too large, particularly at shorter periods. When the distortion parameters are fit only to impedances for $T > 1$ day, the misfits at these long periods are very near their expected values (open circles). The misfits obtained for shorter periods, using the distortion parameters fit to long period impedances, are now significantly larger (asterisks). This demonstrates that the distortion parameters depend at least weakly on period.

derived by distorting Z_0 is smoother than the measured impedance and, within the limits of the distortion model, can be useful when a stable estimate of the full impedance tensor is required for prediction of the electric channels or for cleaning up isolated outliers in the time domain. This might be particularly useful for Z_{xy} and Z_{yy} which are poorly determined at periods longer than about 1 day because of the low amplitude of east-west source fields. We did not make use of this possible refinement for the results discussed in this section, because we did not want to introduce an assumption about the structure prior to testing the adequacy of the distorted one-dimensional model. Subsequent efforts to improve the prediction of missing data based on this idea resulted in negligible changes in the final impedance estimates.

A more quantitative assessment of model fit is possible. The complex quadratic forms $\mathbf{J}_k$ in (8) are weighted sums of squared residuals for each period. These statistics can thus be used to test the goodness of fit of the distorted scalar impedance model as a function of period. If the model (7) is valid (and if the estimation errors are Gaussian), $2\mathbf{J}_k$ is approximately a χ^2 random variable with six degrees of freedom (see the appendix). The expected value of $\mathbf{J}_k$ is thus 3. Typical misfits are actually somewhat larger (solid circles, Figure 13), indicating a small, but statistically significant, failure of the distortion model. It could be argued that this reflects a systematic underestimate of the magnitude of the errors used to normalize (8) [cf., *Chave and Thomson*, 1989; *Jones et al.*, 1989]. However, the complex residuals plotted for each component separately in Figure 14 clearly vary systematically with period. This implies that there is further structure in the full impedance tensors which cannot be fit by the period-independent distortion model. We note that it is straightforward to extend the distorted one-dimensional model to allow for deep two-dimensional structure (*Bahr* [1983]; *Zhang et al.* [1987]; *Groom and Bailey* [1989]; *Smith* [1989]). However, for the Tucson impedances, this more complicated model does not provide a significantly better fit than the distorted one-dimensional impedance model.

Figure 14 suggests that the misfit is systematically larger at shorter periods, and thus a better estimate of the long period, truly static distortion might be obtained by omitting the shorter-period impedance estimates. When the distortion parameters are fit only to impedances with $T > 1$ day, the misfits for these longer periods are very near their expected values (open circles, Figure 13), while the misfits for shorter periods ($T < 1$ day) become much larger (asterisks, Figure 13). This provides some support for the hypothesis that the deeper structure can be adequately modeled as one-dimensional, while lateral conductivity variations at shallower depths still respond inductively at the shorter periods, resulting in a nonstatic distortion. However, it should be kept in

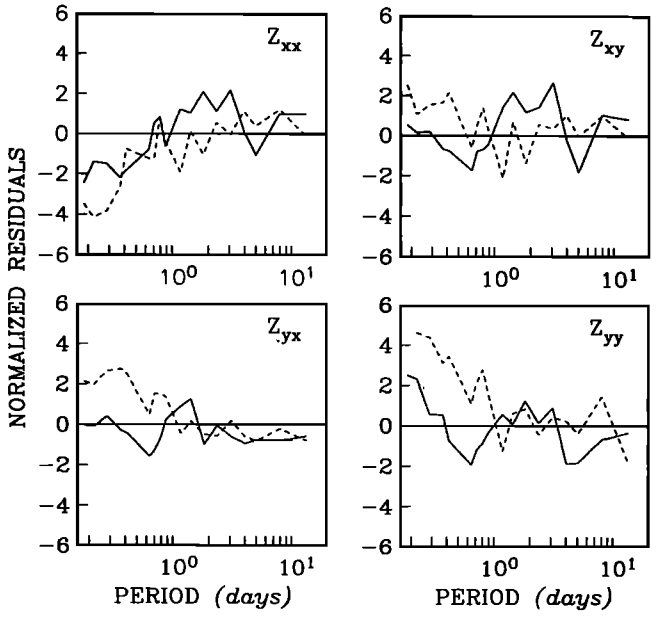

Fig. 14. Normalized residuals from distorted one-dimensional model fit. Solid lines are real parts; dashed lines are imaginary. The residuals are normalized by dividing by the impedance estimation errors (and so should be of order 1 if the distorted scalar impedance model fits adequately). The residuals show a systematic variation with period, implying a significant nonrandom component in the misfit to this simple model.

mind that the relative estimation errors for the impedance elements become larger at longer periods, making the model easier to fit and subtle multidimensional effects more difficult to detect.

6. ONE-DIMENSIONALITY AND THE DISTORTION SCALE

To further explore the consistency of the Tucson MT data set with a one-dimensional conductivity model we applied the D^+ inversion of *Parker* [1980] and *Parker and Whaler* [1981] to the estimated scalar impedances $Z_0(T_k)$. Although D^+ is a physically unlikely conductivity model consisting of a series of delta functions, it achieves the smallest possible value of the χ^2 misfit statistic. These minimum values ($\chi^2_{\min}$) are given in Table 1 for the full MT data set and for three subsets. If the data are one-dimensional, they should have $\chi^2_{\min}$ comparable to or smaller than the expected value of χ^2, which in this case is very close to the number of independent data (*df*). We can conclude that the full data set is not even approximately consistent with any one-dimensional conductivity. Eliminating the shorter periods helps, but none of the subsets tested are unambiguously consistent with one-dimensional structure.

We now estimate the absolute scale, $d = D_{12}$, of the distortion matrix. Assuming that the magnetic fields are not significantly affected by near-surface conductivity variations, that the deep conductivity of the Earth is approximately one-dimensional, and that for sufficiently long periods the external magnetic source potential can be adequately approximated as a zonal geomagnetic dipole (i.e., a P_1^0 spherical harmonic [*Banks*, 1969; *Schultz and Larsen*, 1983]), H_z/H_x transfer functions (relating the vertical and north geomagnetic field components) can be used to obtain undistorted estimates of the long-period one-dimensional MT impedance [e.g., *Larsen*, 1980; *Schultz and Larsen*, 1987]. The distortion scale can then be chosen so that the undistorted MT impedance magnitudes agree with those obtained from the long-period magnetic observatory data. A consistency test is provided by the requirement that phases must be the identical (within their errors) for the two types of data.

We computed robust long-period equivalent MT impedances using 46 years of hourly mean values of magnetic fields (1911-1956) from the Tucson observatory in a manner very similar to that already described for the MT data. Results are plotted as apparent resistivity and phase in Figure 15. The MT and geomagnetic phase curves are reasonably consistent only for periods of 5-10 days. For longer periods, the MT results have large errors and are unreliable, while for shorter periods the phase of the H_z/H_x impedance drops off quickly, presumably due to the breakdown of the P_1^0 source assumption (which is reasonable only for periods longer than 5 days; [*Banks*, 1969; *Schultz and Larsen*, 1983]. The H_z/H_x impedances with $T > 5.0$ days can easily be fit with a one-dimensional model ($\chi^2_{\min} = 6.4$; $df = 18$) and lie very close to the globally averaged apparent resistivity curve given by *Berdichevsky and Zhdanov* [1984]. We therefore joined the MT and H_z/H_x results at a period of 5 days; shorter periods are obtained from MT and longer periods from the H_z/H_x.

TABLE 1. Minimum Achievable Normalized Squared Misfit ($\chi^2_{\min}$) for Four Subsets of the MT Data

Period Range, days	df	$\chi^2_{\min}$
0.17-13.3	36	428
0.50-13.3	26	109
1.00-13.3	18	39
0.11-0.50	16	310

The column denoted df gives the number of degrees of freedom for the χ^2 misfit statistic.

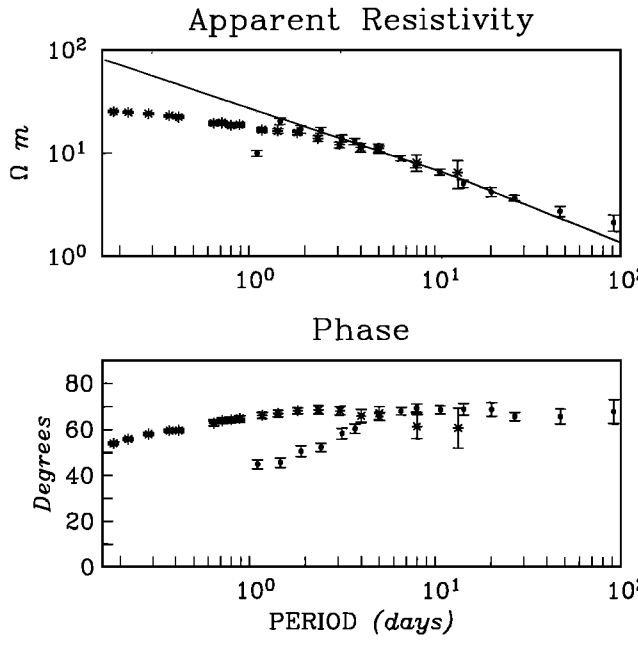

Fig. 15. Apparent resistivities and phases computed from magnetotelluric (asterisks) and H_z/H_x (solid dots) data sets. With an appropriate choice of distortion scale (see text for details) the two data sets are consistent for periods of 5-10 days. For comparison, the global average apparent resistivity curve given by *Berdichevsky and Zhdanov* [1984; p. 43] is plotted as a solid line.

We then computed undistorted MT impedances using a range of possible values for the scale d, merged the rescaled MT impedances with the equivalent H_z/H_x results, and used D^+ to compute the minimum misfit achievable for the combined data set as a function of d. The preferred distortion parameter was chosen to minimize $\chi^2_{\min}(d)$, so that the one-dimensional consistency of the merged data set is optimized. Since the short-period MT data by themselves are not reasonably consistent with a one-dimensional model, we have chosen the distortion scale using only MT impedances for longer periods. To assess the sensitivity of the estimated distortion parameter to the particular choice of long-period cutoff, minimum misfit curves were computed for several period ranges (Figure 16). Our preferred estimate is 2.3, which minimizes the bottom curve (based on periods longer than one day). Although it is difficult to be rigorously quantitative, Figure 16 suggests that the uncertainty in the distortion scale is of the order of ±10%. Changes of this order from the optimum value result in relatively small changes in $\chi^2_{\min}$.

Together the MT and H_z/H_x data provide estimates of the impedance at 24 periods ($T = 0.17$–91 days; Figure 15; Table 2). The consistency of various subsets of these impedances with the one-dimensional conductivity assumption is summarized in Table 3. Since the nine H_z/H_x impedances ($T = 5.0$–91 days) are easily fit with a one-dimensional model, the 15 MT impedances effectively control the achievable misfit of the combined data, and the conclusions for the MT data set by itself still hold: impedances restricted to periods longer than one day are nearly (but not quite) consistent with the one-dimensional assumption; including impedances for shorter periods results in large increases in $\chi^2_{\min}$.

If, however, one inverts apparent resistivity (ρ) or phase (ϕ) separately, one finds that either type of data by itself is consistent with a one-dimensional model over the full bandwidth. The responses for the D^+ models for the complete, combined data and

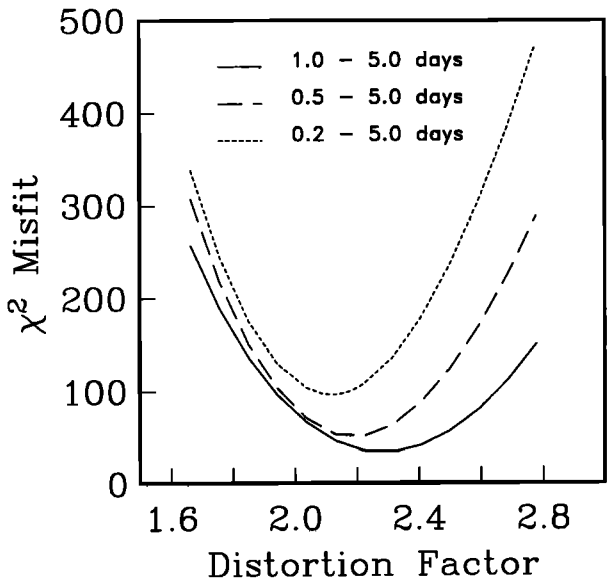

Fig. 16. Minimum misfit achieved by D^+ inversion for combined magnetotelluric and H_z/H_x data as a function of magnetotelluric distortion scale ($\chi^2_{min}(d)$). We take the argument which minimizes $\chi^2_{min}(d)$ as the optimum distortion scale. Results for three different period ranges are plotted. Because the short-period data are inconsistent with any one-dimensional model, our preferred estimate (2.3) is obtained from the bottom curve ($T > 1$ day).

TABLE 2. Apparent Resistivities and Phases for Combined Undistorted MT and Z/H Data Set, With 1σ Error Bars

T, days	ρ, ohm m	σ_ρ, ohm m	φ, degrees	σ_ϕ, degrees	c	ρ_u, ohm m
0.19	25.41	0.27	54.0	0.3	5.40	34.3
0.22	24.86	0.28	55.8	0.3	4.84	30.7
0.29	24.25	0.27	58.0	0.3	4.99	29.3
0.37	23.15	0.24	59.5	0.3	4.04	27.3
0.42	22.35	0.30	59.5	0.4	3.21	26.3
0.65	19.56	0.37	62.7	0.5	2.66	23.7
0.71	19.90	0.40	63.9	0.6	3.09	25.1
0.80	18.47	0.35	64.1	0.5	2.29	22.3
0.89	18.83	0.41	64.6	0.6	1.63	22.7
1.18	16.79	0.38	66.1	0.7	1.38	-
1.43	16.41	0.41	66.9	0.7	1.20	-
1.82	15.78	0.37	68.1	0.7	1.20	-
2.35	13.86	0.44	68.5	0.9	1.20	-
3.08	12.02	0.40	68.1	1.0	1.20	-
4.00	11.27	0.55	65.8	1.4	1.20	-
5.00	11.07	0.57	67.0	1.5	1.20	-
6.56	8.85	0.25	67.8	0.8	1.00	-
7.94	7.64	0.24	69.2	0.9	1.00	-
10.67	6.53	0.21	68.5	0.9	1.00	-
14.22	5.02	0.21	68.7	1.2	1.00	-
20.08	4.20	0.21	68.7	1.5	1.00	-
26.77	3.64	0.11	65.5	0.9	1.00	-
47.08	2.72	0.16	65.6	1.6	1.00	-
91.02	2.12	0.20	67.8	2.6	1.00	-

For $T \leq 5$ days MT results are used; for longer periods Z/H. The column (c) gives the rms normalized misfit of the distorted scalar impedance model (as plotted in figure 13), smoothed over frequency. This is the factor by which impedance errors for each frequency would have to be increased to allow the distorted scalar impedance model to achieve the expected misfit. We take this to be a rough estimate (or perhaps better, lower bound) on the amount error bars should be increased to allow for "geologic noise" when considering a one-dimensional interpretation as we do here. The last column (ρ_u) gives the upward biased apparent resistivity estimates for periods less than one day.

for the inversions of ρ and φ separately are shown in Figure 17. The error bars for the observed responses in this figure have been increased sufficiently (relative to Figure 15) to make all the data pass the one-dimensionality test of Figure 13 (see Table 2 for details). Even with these larger errors, the D^+ response for the combined data still deviates systematically from the estimates of both ρ and φ. Furthermore, the response for the inversion of apparent resistivity only does not fit the phases and vice versa. For a one-dimensional model, ρ and φ should be related via the Hilbert transform [e.g., *Weidelt*, 1972]. It is clear from Figure 17, however, that the observed apparent resistivities are too low ($T < 1$ day) and their slope too shallow ($T < 4$ days) for the observed phase, or alternatively, the observed phases are too high ($0.6 < T < 4$ days) and their slope much too steep ($T < 1$ day) for the observed apparent resistivities. This demonstrates conclusively that the large values of χ^2_{min} for inversion of ρ and φ together do not primarily reflect excessively noisy impedance estimates with overly optimistic error bars (although it is possible that the error bars reported here are slightly too small [see *Chave and Thomson*, 1989; *Jones et al.*, 1989]. Instead, the deviation of the estimated impedances from an acceptable one-dimensional form is smooth, broadband, and systematic, and reflects mainly the failure of ρ and φ to satisfy the Hilbert transform relation implied by causality. Discrepancies of this sort have been noted previously in long-period ocean bottom MT data [*Wannamaker et al.*, 1989; A. Chave, personal communication, 1990], without a satisfactory explanation.

In our case, there are several possible explanations for the discrepancies between ρ and φ. First, they may represent some sort of systematic bias error. The statistical model (1) assumes that noise is confined to the electric field. Noise in the magnetic field channels would result in a downward bias of the ρ curve. Upward biased estimates [e.g., *Jones et al.*, 1989], based on the assumption that all of the noise is in the magnetic fields, are plotted as solid circles in Figure 17*a* for $T < 1$ day. Clearly, this bias could at least contribute to the observed inconsistency between ρ and φ. One could, in principle, remove this bias using a magnetic remote reference. Attempts to do this were not particularly successful, because we were unable to find an observatory that is sufficiently coherent with the Tucson signal to produce estimates with good precision for shorter ($T < 1$ day) periods.

Another possibility is that source structure effects have produced an upward bias of φ. We have shown that phases are systematically biased upward at periods near harmonics of the S_{dv}. It is at least possible that phase biases, while most extreme at S_{dv} periods, also affect intermediate periods. Geomagnetic storms and substorms have finite spatial scales, and while the resulting D_{st} fields are certainly more random than S_q fields, they exhibit a certain amount of regularity (e.g., on average disturbances propagate from east to west [*Rostoker*, 1972; *Banister and Gough*,

TABLE 3. Minimum Achievable Normalized Squared Misfit (χ^2_{min}) for Seven Subsets of the Combined MT and Z/H data

Data Set	df	χ^2_{min}
ρ and φ: 0.16 - 90. days	48	566
ρ and φ: 0.50 - 90. days	38	127
ρ and φ: 1.00 - 90. days	30	44
ρ and φ: 5.00 - 90. days	18	6.4
ρ only: 0.16 - 90. days	24	24
φ only: 0.16 - 90. days	24	12
upward biased ρ, errors increased	48	62

Data subsets are discussed in text. The column denoted df gives the number of degrees of freedom for the χ^2 misfit statistic.

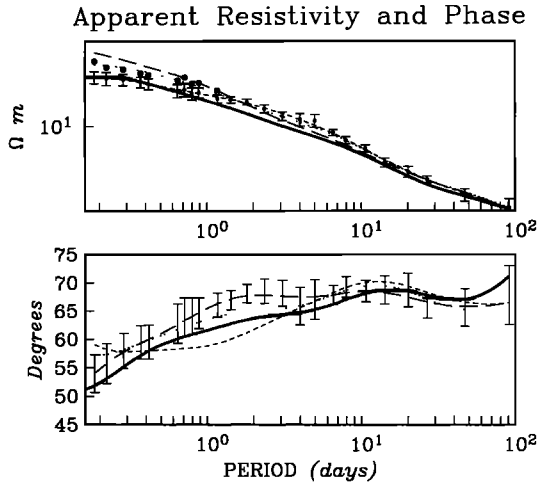

Fig. 17. Estimated apparent resistivity and phase for some best fitting (D^+) one-dimensional models. In this plot, error bars for periods less than one day have been increased to reflect the magnitude of the misfit of the distorted scalar impedance model (see note to Table 2). The solid dots represent upward biased apparent resistivity estimates obtained under the assumption that all of the noise is in the magnetic fields, while the apparent resistivities plotted with error bars represent the usual (downward biased) magnetic field reference estimates. The four model responses plotted are as follows. Heavy solid line is best fit to all data. Long-dashed line is best fit to phase only. Short-dashed line is best fit to apparent resistivity only. For these three models the original estimation errors were used to normalize the misfit. For the model response represented by the dotted line we replaced apparent resistivities for periods less than one day with the upward biased estimates, and we used the increased error bars (as plotted here) to normalize the misfit.

1978]). As a consequence we should not expect the continuum of geomagnetic variations to average exactly to an effectively uniform source. It is probably more likely that our impedances correspond to an average source with finite spatial scale which tends to move from east to west. Given the evidence for systematic phase variations of the order of 5–10° at S_{dv} periods, upward biases of phases (relative to those produced by uniform sources) of at least a few degrees do not seem implausible.

Finally, it is possible that the inconsistency between ρ and φ results from lateral variations of conductivity not accounted for by the static distortion model. A complex three-dimensional MT response need not be consistent with any one-dimensional model [*Egbert*, 1990; *Svetov*, 1990]. *Swift* [1967] provides evidence (from higher frequency MT data) for lateral conductivity variations in the lower crust or uppermost mantle beneath the southwestern United States. Although these relatively shallow features appear as static distortion for low enough frequencies, they may possibly complicate a one-dimensional interpretation at the upper end of our frequency range. The increased errors in Figure 17, which are the minimum required for the statistical consistency of the distortion model (6), represent a minimum estimate of this "geologic noise." We have seen, however, that these increased errors were not large enough to make the combined data set consistent with one-dimensionality in the D^+ sense or resolve the discrepancy between apparent resistivity and phase. However, if one uses the upward-biased estimates of ρ for $T < 1$ day and the adjusted errors, one can find a D^+ model which is nearly consistent with all the modified data (dotted line, Figure 17; Table 3). Thus in combination, relatively small systematic biases and subtle multidimensional complications can almost certainly explain the observed deviations of the Tucson data from one-dimensionality.

7. DISCUSSION

The elements of the distortion matrix **D** are given in geographic coordinates in Table 4. The columns of **D** represent the distorted electric field vectors resulting from unit magnitude undistorted electric fields polarized east-west and north-south, respectively. For both polarizations the distorted fields are amplified and rotated toward the northeast. As a consequence, geomagnetic north-south sources which are dominant at long periods produce electric fields of comparable amplitude in both the north and east directions. This is why the signal-to-noise ratios, as estimated by the multiple coherences (Figure 7), are comparable for both electric field components.

The directions of maximum and minimum electric field distortion are given by the eigenvectors of the 2×2 matrix **D**. These principal directions are plotted on both the large-scale map in Figure 1 and a simplified regional geology map in Figure 18. The eigenvectors are scaled by the corresponding eigenvalues of **D** which give the magnitudes d_{max} and d_{min} of maximum and minimum stretching of the electric fields. This distortion is dominated by strong amplification (by a factor of 3.88) in a direction 42° east of north. The minimum distortion (1.12) occurs in a direction 17° west of north.

It is clear from Figure 1 that the principle direction of distortion is roughly perpendicular to the continental margin. The coast is a contact between a conductive and resistive surface. Continuity of current requires amplified electric fields perpendicular to the coast on the continent. However, several lines of evidence suggest that the ocean probably does not have a significant effect on the electric fields as far inland as Tucson. As discussed by *Ranganayaki and Madden* [1980] and *Mackie et al.* [1988], electric currents induced in the highly conducting ocean which cross the coast, leak down to an aesthenospheric good conductor over a characteristic length scale determined by the transverse resistance (thickness/conductivity) of the lithosphere. We have computed responses for two-dimensional models including the ocean and Gulf of California. (Three-dimensionality will weaken distortion due to the coast.) To reproduce the amplitude of the electric field distortion observed across the Tucson dipoles, 650 km from the ocean, we find that a lower crustal resistance of several times 10^9 ohm m^2 is required. In fact, this is comparable to values of crustal resistance that have been estimated from controlled source electromagnetic experiments on the seafloor [*Cox et al.*, 1986]; from a long-period ($T < 1$ day) MT site near Holister, California [*Mackie et al.*, 1988], and from a global scale analysis of vertical electric current flow induced by S_q fields [*Fainberg et al.*, 1990]. However, our modeling results also demonstrate that the resistive layer must be continuous. Even small, moderately conductive breaks in the resistive zone can short the oceanic currents to the deeper conductor and result in rapid attenuation of the oceanic electric fields. We consider it unlikely that a sufficiently resistive and continuous layer exists across the continental margin, the East Pacific Rise, and into the Basin and Range.

Experimental evidence supports this view. *Park et al.* [1991] found that oceanic electric fields, clearly evident in the California

TABLE 4. Electric Field Distortion Tensor Elements in Geographic Coordinates

	North	East
North	1.82	2.24
East	0.63	3.23

The two columns give the distorted electric field vectors resulting from unit magnitude undistorted electric fields in the north and east directions.

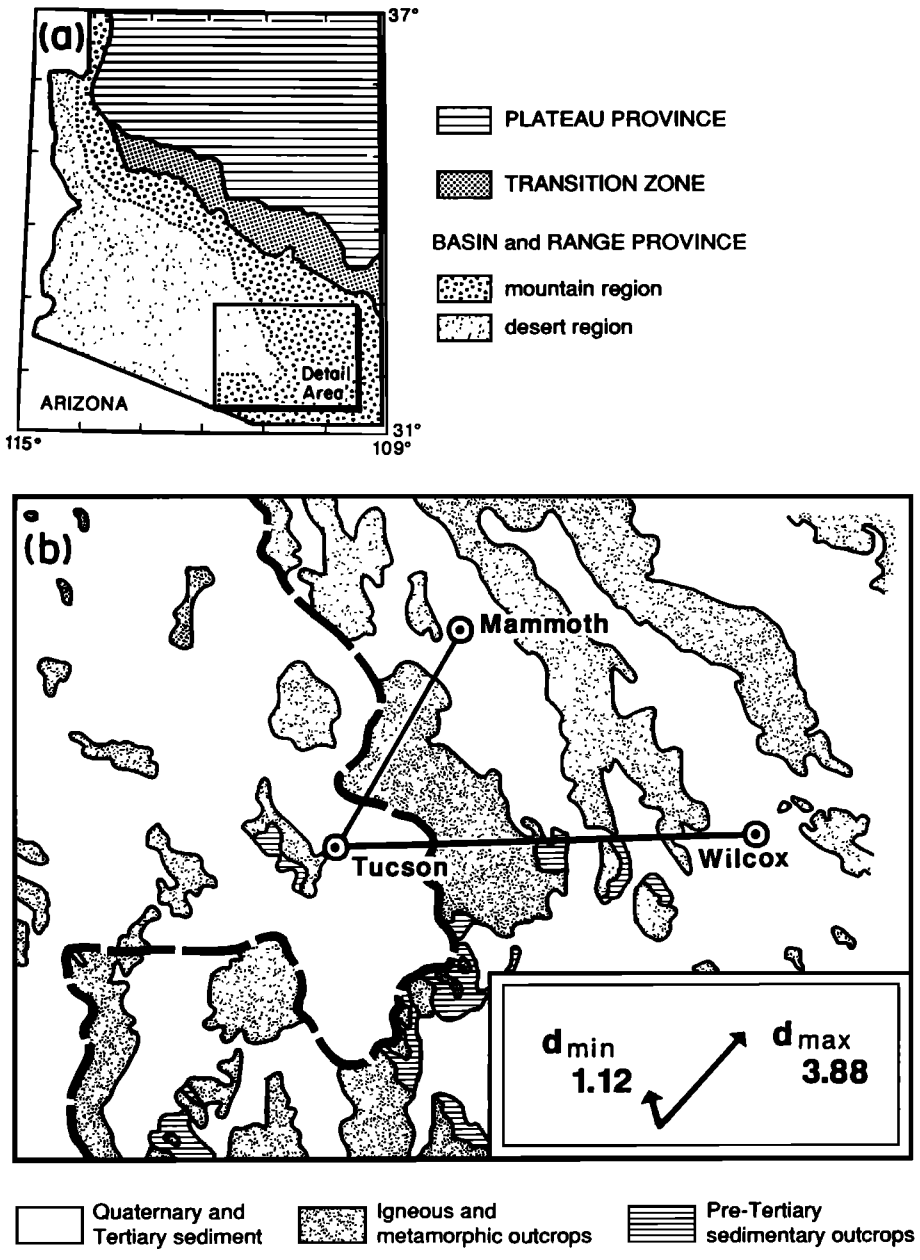

Fig. 18. (*a*) Physiographic provinces in the state of Arizona. The electric field receiver dipoles lie within the basin and range province but straddle the edge of the desert and mountain regions within this province. (*b*) Simplified surface geology map of the Tucson area, showing electrode locations and the boundary between the desert and mountain regions. In the mountain region the outcropping ranges rise higher above the interconnected basins and have longer strikes. As a consequence the large-scale average transverse resistance of the surface layer is higher in the mountain region, particularly in the direction perpendicular to the ranges. Note that while the electrodes are all located within the sedimentary basins, the receiver dipoles straddle a relatively continuous NNE trending resistive range. Principal directions and eigenvalues of electric field distortion tensor are inset in the lower right hand corner. The direction of maximum magnification of the electric fields is roughly perpendicular to the regional strike of the basins and ranges. In the direction parallel to the strike of surface features, the electric field is almost undistorted.

Coast Range, were completely dissipated on the eastern edge of the San Joaquin Valley. Furthermore, MT sites across the Basin and Range/Southern Colorado Plateau transition zone, near Flagstaff, Arizona, (300 km north of Tucson) show no evidence of oceanic influence [*Klein*, 1991], and recent MT data taken in the Chocolate Mountains along the PACE transect in southeastern California (slightly north, but well to the west of Tucson) also show no evidence of oceanic effects (G. Jiracek and S. Park, personal communication, 1990). Finally, our analysis of noise at tidal periods (see Figure 8) indicates that tidally induced electric fields are not significant at Tucson. We thus believe that the ocean has little effect on the electric fields measured at Tucson and that the observed distortion results from more local near-surface conductivity variations.

There is ample reason to believe that the near-surface structure in the vicinity of Tucson can explain the observed distortion. From Figure 18, one can see that the maximum distortion is also perpendicular to the regional strike of the southern Basin and Range province (BR), which is characterized by relatively resistive ranges rising above conducting basins [e.g., *Wannamaker*,

1983; *Klein*, 1991]. The minimum distortion is approximately along strike. In the desert region of the southern BR, the resistive ridges are isolated islands in conductive surface sediments. In the mountain region north and east of Tucson, the resistive ridges dominate and the sediment filled valleys are more isolated. Thus, on the large scale, the surface resistance of the desert region should be substantially lower than the mountain region. The electric field receiver dipoles lie primarily in the mountain region and are thus on the resistive side of a large-scale contact. Again, one expects that the electric field on the resistive side will be amplified perpendicular to the contact. This amplification will be further increased by the fact that the dipoles straddle resistive ridges which are elongated parallel to the larger-scale contact.

Our estimate of the distortion of the Tucson electric fields is of historical interest. *Tikhonov* [1950] inferred from the Tucson data that the mantle was relatively resistive, (hundreds of ohm m) to depths of 950 km. *Price* [1962] pointed out that these results were at variance with conductivity profiles determined from spherical harmonic analysis of magnetic variations [*Lahiri and Price*, 1939], and argued that the discrepancy reflected the failure of the uniform source assumption which justifies the MT method. Tikhonov's impedance estimate was based on the ratio, at S_{dv} periods, of the geomagnetic north electric to geomagnetic east magnetic components, and of course he was unaware of the possibility of electric field distortion. For his coordinate system, the electric field is amplified by a factor of 2.34. Applying this correction to Tikhonov's results yields an estimated depth to the top of the conductor of 400 km, in much better agreement with the magnetic variation results. As *Madden and Nelson* [1986] pointed out at the time, the major difficulty in the application of the MT method lies in complications arising from lateral conductivity variations not from source effects.

Finally, the conductance profiles

$$S(z) = \int_0^z dz' \sigma(z') ,$$

for the D^+ models corresponding to the various inversions discussed in connection with Figure 17 are plotted in Figure 19. As discussed by *Weidelt* [1985], determining $S(z)$ from estimates of ρ and ϕ is a well-posed problem. All conductivity profiles which produce similar ρ and ϕ curves will be similar (in a manner which can be made mathematically precise). Thus the D^+ conductance profiles provide direct insight into the vertically averaged conductivity structure of the Earth. First, and most importantly, all the profiles are very similar. This gives us some confidence that inferences about gross features of the true $S(z)$ are relatively insensitive to the manner in which we resolve the phase and amplitude inconsistency. In all cases, $S(z)$ reaches values of roughly 10^4 Siemens (S) by 150 km depth, 10^5 S at around 400 km, and 10^6 S by 1000 km. Further increases (to several times 10^7 S) occur near 2000 km depth, beyond the depth where our data is useful. This implies already that the large scale average conductivities must be of the order of 0.05 S m^{-1} in the first 200 km, increasing to 0.2 S m^{-1} or more between 200 and 700 km depth, and finally to roughly 1.0 S m^{-1} by around 1000-1500 km. These rough calculations are valid for all four of the D^+ models of Figure 19. A more detailed discussion of the implications of these data for mantle conductivity are presented in a companion paper [*Egbert and Booker*, this issue].

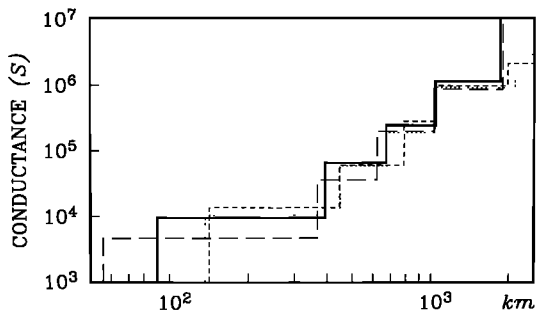

Fig. 19. Conductance profiles corresponding to the D^+ models of Figure 17. The profiles are similar, indicating that conclusions based on one-dimensional modeling of the data will be relatively insensitive to the manner in which we resolve the inconsistency between the phase and apparent resistivity curves.

8. CONCLUSIONS

The Tucson data, from one of the very first MT experiments ever conducted, yield impedance estimates in the period range $0.17 < T < 10$ days of unparalleled precision. The high quality of these results can be attributed to the very long electrode lines and the long duration of the experiment. At the longest periods ($T > 10$ days) the electric fields recorded at Tucson are dominated by noise. At shorter periods ($T < 1$ day) we have found clear evidence that finite spatial scale sources can cause small systematic biases in the MT impedances, particularly at harmonics of the fundamental daily variation period. The possibility that such biases might occur at intermediate periods cannot be completely dismissed. Further research to clarify this issue is warranted.

The full set of Tucson impedance tensors are very nearly equal to the product of a complex scalar (period dependent) impedance and a single (period independent) real distortion matrix, suggesting a deep one-dimensional conductivity distribution complicated by near-surface lateral variations. The distortion is consistent with regional variations in surface geology. However, the phase and amplitude of the resulting scalar impedance are not jointly consistent with any one-dimensional conductivity model. This discrepancy may result from systematic biases in the estimated impedances (possibly including source effects) or from multidimensional complications. The discrepancy is much greater than the statistical estimation errors and thus substantially reduces the resolving power of the short-period MT data.

It is tempting to suggest that much better MT data could be obtained, particularly at very long periods, with modern instruments. However, this is not completely clear. To the extent that long-period noise represents drift due to slow changes in the electrochemical environment of the electrodes, long-period results should be substantially improved by collecting MT data in a very stable environment, such as in freshwater lakes [*Schultz et al.*, 1987]. However, the origin of the long-period noise seen in the Tucson data is unclear. Variations of electrochemical self-potential fields in the crust, streaming potentials due to subsurface water flow, piezoelectric effects, and variations of near-surface resistivity with time could all contribute to long-period "noise." It is important to realize that the MT impedance decreases rapidly, and electric field signal amplitudes become very small, at long periods (at $T = 100$ days the impedance is a factor of 30 smaller than at $T = 1$ day). As a consequence, subtle sources of crustal electric fields which are negligible at shorter periods may come to dominate the signal at long periods. A very long-period MT experiment using instruments which essentially eliminate electrode drift problems [*Filloux*, 1974] is now underway and may shed some light on the possible nature of long-period electric field signal and noise [*Schultz et al.*, 1991].

Whether or not substantially more precise very long-period MT impedance estimates can be obtained in the future, it is worth bearing in mind that systematic biases, source complications, and multidimensional effects limit our ability to interpret the Tucson data more than noise in the estimates. These complications will probably present the primary impediment to further progress on the question of mantle conductivity.

APPENDIX: ESTIMATION OF DISTORTION PARAMETERS

In this appendix we briefly discuss our approach to estimation of the static distortion parameters $\mathbf{d}$ and the undistorted scalar impedances $Z_0(T_k)$, $k = 1, K$. Using the notation defined in section 5, and assuming the model of (7), we seek to minimize the weighted residual sum of squares of (8), reproduced here:

$$\mathbf{J} = \sum_k \mathbf{J}_k = \sum_k (\mathbf{z}_k - \mathbf{d}Z_0(\omega_k))^\dagger \Sigma_k^{-1} (\mathbf{z}_k - \mathbf{d}Z_0(\omega_k)) \ . \qquad (8')$$

This represents a nonlinear least squares problem which can be solved by several means (e.g., by use of a Newton-Rapheson method to solve the corresponding nonlinear normal equations). We have used an alternative approach based on an iterative conditional least squares method. With the distortion parameters fixed, (8′) reduces to a series of decoupled linear least squares problems. Thus for fixed $\mathbf{d}$ the estimates of the scalar impedances $\hat{Z}_0(T_k)$ which minimize $\mathbf{J}$ can be found by minimizing the quadratic forms $\mathbf{J}_k$ separately. This is a straightforward linear least squares problem with solution

$$\hat{Z}_0(\omega_k) = (\mathbf{d}^\dagger \Sigma_k^{-1} \mathbf{d})^{-1} \mathbf{d}^T \Sigma_k^{-1} \hat{\mathbf{z}}_k \qquad (A1)$$

On the other hand, with the scalar impedances $Z_0(T_k)$ fixed, (8′) represents a linear least squares problem for the real distortion parameters $\mathbf{d}$. The solution to this problem may be written in terms of the complex impedances and error covariance matrices as

$$\hat{\mathbf{d}} = \left[\sum_{k=1}^{K} |Z_0(T_k)|^2 \mathrm{Re}(\Sigma_k)^{-1} \right]^{-1} \sum_{k=1}^{K} \mathrm{Re}\left[Z_0(T_k)^* \Sigma_k^{-1} \hat{\mathbf{z}}_k \right] \qquad (A2)$$

This suggests a simple iterative estimation procedure: begin with a simple estimate of the undistorted scalar impedance (e.g., $\hat{Z}_{12}(\omega_k)$) and then using (A2) and (A1) alternately improve the estimates of the distortion parameters, and the one-dimensional impedances. It is readily shown that this iterative approach reduces the misfit $\mathbf{J}$ at every step and hence always converges to a (local) minimum of $\mathbf{J}$. Note that with this estimation approach the absolute scale of the distortion parameters is arbitrary. This scale must be determined using other information. An application of this general estimation method (to a very different problem) is described in greater detail by *Egbert* [1991].

The iterative least squares scheme suggests a simple approximate estimate of standard errors for the undistorted impedances. If the distortion parameters were known the estimate at period T_k would be the weighted least squares estimate of (A1) with error variance

$$Var[\hat{\mathbf{Z}}(\omega_k)] = \mathbf{d}^T \Sigma_k \mathbf{d} \ . \qquad (A3)$$

Furthermore, if the model is correct (and if the estimation errors are Gaussian), the total normalized squared misfit at frequency ω_k given by the complex quadratic form

$$2\mathbf{J}_k = 2(\mathbf{z}_k - \mathbf{d}Z_0(\omega_k))^\dagger \Sigma_k^{-1} (\mathbf{z}_k - \mathbf{d}Z_0(\omega_k)) \qquad (A4)$$

is a χ^2 random variable with six degrees of freedom which can be used to test for goodness of fit of the distorted one-dimensional model as a function of frequency.

Since the distortion parameters $\mathbf{d}$ are also estimated, the estimation variance given in (A3) is not exactly correct, and the distribution of the goodness-of-fit statistics $\mathbf{J}_k$ should be modified slightly. The general results derived by *Egbert* [1991; Appendix C] can be used to compute a large sample approximation to the covariance matrix of the scalar impedance estimates. For the problem considered here this further analysis results in only a small refinement of the much simpler expression of (A3), so we only indicate the form of the correction for a simple but illustrative special case. Assuming for simplicity of discussion that the error covariance matrices are diagonal $\Sigma_k = \sigma_k^2 \mathbf{I}$, the error variance for the real and imaginary parts of $Z_0(T_k)$ calculated from (A3) are each $\frac{1}{2}\sigma_k^2 |\mathbf{d}|^2$. Using the more refined asymptotic analysis of *Egbert* [1991], the error variance for the real part of $Z_0(T_k)$ is found to be approximately $\frac{1}{2}\sigma_k^2 |\mathbf{d}|^2 (1 - w_{Rk}^2)^{-1}$, where

$$w_{Rk}^2 = \frac{[\mathrm{Re}\, Z_0(T_k)]^2 \sigma_k^{-2}}{\sum_{k=1}^{K} |Z_0(T_k)|^2 \sigma_k^{-2}} \qquad (A5)$$

Analogous correction factors for the imaginary parts w_{Ik}^2 are obtained by replacing $\mathrm{Re}\, Z_0(T_k)$ by $\mathrm{Im}\, Z_0(T_k)$ in (A5).

In general,

$$\sum_{k=1}^{K} w_{Rk}^2 + w_{Ik}^2 = 1.$$

Thus when the number of frequency bands K is large, $w_{Rk}^2, w_{Ik}^2 \ll 1$ and the simple expressions given in (A3) should be adequate. For the Tucson data (with K of order 20) the refined asymptotic variances are only a few percent larger than the variances obtained from (A3). Corrections to the expected value of the residual statistics $\mathbf{J}_k$ are of similar order. Considering the other uncertainties (e.g., concerning error distributions or systematic biases) we consider the simple approximate expressions of (A3) and (A4) to be adequate.

Acknowledgments. J. C. Larsen provided much of the inspiration for the analysis reported here, as well as a copy of the Tucson electric field data. T. Zhang assisted in the early phase of this work. Support was provided by the National Science Foundation through grant EAR-8708401 and for one of us (G.E.) by the Department of Energy through grant DOE-FG06-89ER14057.

REFERENCES

Bahr, K., Joint interpretation of magnetotelluric and geomagnetic depth sounding data and local telluric disturbances, *J. Geomagn. Geoelectr.*, *35*, 555-566, 1983.

Banks, R.J., Geomagnetic variations and the electrical conductivity of the upper mantle, *Geophys. J. R. Astron. Soc.*, *17*, 457-487, 1969.

Banks, R.J., and M. Ainsworth, Global induction and the spatial structure of mid-latitude geomgnetic variations, *Geophys. J. Int.*, in press, 1992.

Bannister, J.R., and D.I. Gough, A study of two polar magnetic substorms with a two-dimensional magnetometer array, *Geophys. J. R. Astron. Soc.*, *53*, 1-26, 1978.

Berdichevsky, M.N., and M.S. Zhdanov, *Advanced Theory of Deep Geomagnetic Sounding*, 408 pp., Elsevier, New York, 1984.

Chave, A.D., and D.J. Thomson, Some comments on magnetotelluric response function estimation, *J. Geophys. Res.*, *94*, 14,215-14,226, 1989.

Cox, C.S., S.C. Constable, A.D. Chave, and S.C. Webb, Controlled-source electromagnetic sounding of the oceanic lithosphere, *Nature*, *320*, 52-54, 1986.

Dmitriev, V.I., and M.N. Berdichevsky, The fundamental model of magnetotelluric sounding, *Proc. IEEE*, *67*, 1033-1044, 1979.

Egbert, G.D., Multivariate analysis of global magnetometer array data, paper presented at Sixth Scientific Assembly, Int. Assoc. of Geomagn. and Aeron., Exeter, England, July 24 to Aug. 4, 1989.

Egbert, G.D., Comments on "Concerning dispersion relations for the mag-

netotelluric impedance tensor" by E. Yee and K.V. Paulson, *Geophys. J. Int., 102*, 1-8, 1990.

Egbert, G.D., On the synthesis of a large geomagnetic array from small overlapping arrays, *Geophys. Jour. Int., 106*, 37-51, 1991.

Egbert, G.D., Non-causality of the discrete time magnetotelluric impulse response, *Geophysics*, in press, 1992.

Egbert, G., and J.R. Booker, Robust estimation of geomagnetic transfer functions, *Geophys. J. R. Astron. Soc., 87*, 173-194, 1986.

Egbert, G.D., and J.R. Booker, Very long period magnetotellurics at Tucson Observatory: Implications for mantle conductivity, *J. Geophys. Res.*, this issue.

Fainberg, E.B., A.V. Kuvshinov, and B. Sh. Singer, Electromagnetic induction in a spherical earth with non-uniform oceans and continents in electric contact with the underlying medium - II. Bimodal global geomagnetic sounding of the lithosphere, *Geophys. J. Int., 102*, 283-286, 1990.

Filloux, J.H., Electric field recording ob the seafloor with short span instruments, *J. Geomagn. Geoelectr., 26*, 269-279, 1974.

Groom, R.W., and R.C. Bailey, Decomposition of magnetotelluric impedance tensors in the presence of local three-dimensional galvanic distortion, *J. Geophys. Res., 94*, 1913-1925, 1989.

Huber, P.J., *Robust Statistics*, John Wiley, New York, 1981.

Jones, A. G., A.D. Chave, G.D. Egbert, D. Auld, and K. Bahr, A comparison of techniques for magnetotelluric response function estimation, *J. Geophys. Res., 94*, 14,201-14,214, 1989.

Klein, D.P., Crustal resistivity structure from magnetotelluric soundings in the Colorado Plateau-Basin and Range Provinces, central and western Arizona, *J. Geophys. Res., 96*, 12,313-12,332, 1991.

Lahiri, B.N., and A.T. Price, Electromagnetic induction in nonuniform conductors, and the determination of the conductivity of the earth from terrestrial magnetic variations, *Phil. Trans. R. Soc. London, Ser. A, 237*, 509-540, 1939.

Larsen, J.C., Low frequency (0.1-6.0 cpd) electromagnetic study of deep mantle conductivity beneath the Hawaiian Islands. *Geophys. J. R. Astron. Soc., 43*, 17-46, 1975.

Larsen, J.C., Removal of local surface conductivity effects from low frequency mantle response curves, *Acta Geodaet. Geophys. Montanist. Acad. Hung., 12*, 183-186, 1977.

Larsen, J.C., Electromagnetic response functions from interrupted and noisy data, *J. Geomagn. Geoelectr., 32 SI*, 89-103, 1980.

Mackie, R.L., B.R. Bennett, and T.R. Madden. Long period magnetotelluric measurements near the central California coast: a land-locked view of the conductivity structure under the Pacific Ocean, *Geophys. J., 95*, 181-194, 1988.

Madden, T., and P. Nelson, A defense of Cagniard's magnetotelluric method, in *Magnetotelluric Methods*, edited by K. Vozoff, 763 pp., Society of Exploration Geophysicists, Tulsa, Okla., 1986.

Melchior, P., *The Tides of the Planet Earth*, 609 pp., Pergamon, New York, 1978.

Park, S.K., G.P. Biasi, R.L. Mackie, and T.R. Madden, Magnetotelluric evidence for crustal suture zones bounding the southern Great Valley, California, *J. Geophys. Res., 96*, 353-376, 1991.

Parke, M.E., O1, P1, N2 models of the global ocean tide on an elastic earth, plus surface potential and spherical harmonic decompositions for M2, S2, and K1, *Mar. Geod., 6*, 35-81, 1982.

Parker, R.L., The inverse problem of geomagnetic induction: Existence and construction of solutions based upon incomplete data, *J. Geophys. Res., 85*, 4421-4428, 1980.

Parker, R.L. and K.A. Whaler, Numerical methods for establishing solutions to the inverse problem of electromagnetic induction, *J. Geophys. Res., 86*, 9574-9584, 1981.

Price, A.T., The theory of magnetotelluric methods when the source field is considered, *J. Geophys. Res., 67*, 1907-1918, 1962.

Ranganayaki, R.P., and T.R. Madden, Generalized thin sheet analysis in magnetotellurics, an extension of Price's analysis, *Geophys. J. R. Astron. Soc., 60*, 445-457, 1980.

Rooney, W.J., Earth-Current Results at Tucson Magnetic Observatory, 1932-1942, *Res. Dep. of Terr. Magn. Carnegie Inst. Washington, 9*, 307 pp., 1949.

Rostocker, G., Polar magnetic substorms, *Rev. Geophys. Space Phys., 10*, 157-211, 1972.

Schultz, A., and J.C. Larsen, Analysis of zonal field morphology and data quality for a global set of magnetic observatory daily mean values, *J. Geomagn. Geoelectr., 35*, 835-846, 1983.

Schultz, A., and J.C. Larsen, On the electrical conductivity of the earth's interior I: mid-mantle response function computation, *Geophys. J. R. Astron. Soc., 88*, 733-761, 1987.

Schultz, A., J. Booker, and J. Larsen, Lake bottom magnetotellurics, *J. Geophys. Res., 92*, 10,639-10,649, 1987.

Schultz, A., R. Kurtz, A. Chave and A. Jones, Deep conductivity structure beneath the Kapuskasing region: Inferences from a very long period lake bottom magnetotelluric observatory, paper presented at Canadian Geophysical Union Meeting, Banff, Alberta, May 13-17, 1991.

Smith, J.T., Towards realistic errors for 2-d MT inversion, paper presented at 6th Scientific Assembly, Int. Assoc. of Geomagn. and Aeron., Exeter, England, July 24 to Aug. 4, 1989.

Svetov, B.S., About special features of transfer functions of MT-fields, paper presented at 10th Workshop on Electromagnetic Induction in the Earth, Int. Assoc. of Geomagn. and Aeron., Ensenada, Mexico, Aug. 22-29, 1990.

Swift, C.M., A magnetotelluric investigation of an electrical conductivity anomaly in the southwestern United States, Ph.D. dissertation, Mass. Inst. of Technol., Cambridge, 211 pp., 1967.

Thomson, D.J., Spectrum estimation techniques for characterization and development of WT4 waveguide, I, *Bell Syst. Tech. J., 56*, 1769-1815, 1977.

Tikhonov, A.N., Determination of the electrical characteristics of the deep layers of the earth's crust, *Dokl. Akad. Nauk USSR, 73*, 295-297, 1950.

Tikhonov, A.N., and D.N. Shaksuvarov, Concerning the possibility of using the impedance of the earth's natural electromagnetic field for investigating its upper layers, *Izv. Acad. Nauk. SSSR, Ser. Geofiz., 4*, 410-418, 1952.

Waitt, J.R., Theory of magnetotelluric fields, *J. Res. Natl. Bur. Stand., Sect. D, 66*, 509-541, 1962.

Wannamaker, P., Resistivity structure of the northern Basin and Range and its tectonic implications, in *The Role of Heat in the Development of Energy and Mineral Resources in the Northern Basin and Range Province*, 345-362, Geothermal Resources Council, Davis, Calif., 1983.

Wannamaker, P.E., J.R. Booker, A.G. Jones, A.D. Chave, J.H. Filloux, H.S. Waff, and L.K. Law, Resistivity cross section through the Juan de Fuca subduction system and its tectonic implications, *J. Geophys. Res., 94*, 14,127-14,145, 1989.

Weidelt, P., The inverse problem of geomagnetic induction, *Z. Geophys., 38*, 257-289, 1972.

Weidelt, P., Construction of conductance bounds from magnetotelluric impedances, *J. Geophys., 57*, 191-206, 1985.

Zhang, P., R.G. Roberts, and L.B. Pedersen, Magnetotelluric strike rules, *Geophysics, 52*, 267-278, 1987.

J.R. Booker, Geophysics Program AK-50, University of Washington, Seattle WA 98195.

G.D. Egbert, College of Oceanography, Oregon State University, Oceanography Admin. Bldg. 104, Corvallis, OR, 97330-5503.

A. Schultz, Institute of Theoretical Geophysics, Department of Earth Sciences, University of Cambridge, Downing Street, Cambridge CB2 3EQ, England.

(Received July 9, 1991;
revised March 1, 1992;
accepted May 2, 1992.)